International Journal of Energy Research

WILEY

RESEARCH ARTICLE OPEN ACCESS

Accurate Prediction of Thermal Conductivity in Methane Binary Mixtures for Energy Applications Using a Convolutional Neural Network

Sadegh Motahar[1] | Mohammadreza Shams[2] | Mohsen Jannati[3] | Mohammed Saedi Jami[4]

[1]Department of Mechanical Engineering, University of Isfahan, Shahreza Campus, Isfahan, Iran | [2]Department of Computer Engineering, University of Isfahan, Shahreza Campus, Isfahan, Iran | [3]Department of Electrical Engineering, University of Isfahan, Shahreza Campus, Isfahan, Iran | [4]Department of Chemical Engineering and Sustainability, International Islamic University Malaysia, Kuala Lumpur 50728, Malaysia

Correspondence: Sadegh Motahar (s.motahar@shr.ui.ac.ir)

Received: 29 October 2025 | **Revised:** 13 June 2026 | **Accepted:** 1 July 2026

Academic Editor: Arnab Biswas

Keywords: convolutional neural networks (1D-CNNs) | machine learning models | methane binary gas mixtures | thermal conductivity prediction | thermophysical properties

ABSTRACT

Accurate prediction of thermal conductivity in methane (CH_4)-based binary gas mixtures is essential for enhancing the efficiency and safety of energy systems, gas separation processes, and the design of industrial equipment. Conventional empirical and theoretical models often lack sufficient accuracy when dealing with complex, nonlinear molecular interactions and require extensive experimental data. In this study, a novel framework based on one-dimensional convolutional neural networks (1D-CNNs) was developed to predict the thermal conductivity of CH_4 mixtures with seven gases (CO_2, CO, CF_4, H_2, N_2, Ne, and Ar) using fundamental input parameters such as temperature, pressure, and mole fractions. The model architecture was optimized through hyperparameter tuning, root mean square propagation (RMSprop) optimization, and dropout regularization to minimize overfitting while maintaining strong generalization capability. Quantitative evaluation demonstrated that the proposed model significantly outperformed traditional approaches, including random forest regression, feed-forward neural network (FFNN), support vector regression (SVR), and linear regression (LR), achieving $R^2 = 0.995$, mean absolute percentage error (MAPE) = 2.02%, mean absolute error (MAE) = 0.94 mW/m·K, and root mean square error (RMSE) = 1.59 mW/m·K. Residual analyses confirmed the model's excellent agreement with experimental data and minimal prediction bias. The results establish the proposed model as a powerful, scalable, and extensible tool for a wide range of industrial applications, including combustion modeling, thermal management in membrane technologies, cryogenic process design for liquefied natural gas (LNG) systems, and safety analysis of natural gas transmission pipelines.

1 | Introduction

1.1 | Background

Driven by the simultaneous rise in the global population and economic development, the demand for natural resources, particularly fossil fuels, has increased significantly. This growing reliance on fossil fuels, combined with their finite availability, has raised pressing concerns about energy security and environmental sustainability [1]. Among these fuels, methane stands out as one of the most abundant and essential hydrocarbons, playing a vital role in various engineering processes and contributing to global economic growth. As the primary component of natural gas, methane is extensively used across multiple sectors, including electricity generation in thermal power plants, compressed natural gas

(CNG) vehicles, and residential heating systems [2]. Furthermore, it serves as a key feedstock in the production of ammonia, hydrogen, and numerous petrochemical products [3, 4]. However, despite its benefits, methane presents a significant environmental challenge: as the second most prevalent greenhouse gas after carbon dioxide, its emissions can contribute substantially to global warming, resulting in severe ecological consequences. Therefore, the effective control and reduction of methane emissions have become critical priorities in the pursuit of sustainable environmental management and climate change mitigation [5]. This necessity extends beyond environmental considerations; in large-scale industries such as gas transportation systems, liquefied natural gas (LNG) units, and combustion chambers, accurate prediction of methane's thermophysical properties directly influences safety, cost, and operational efficiency.

Accurate prediction and modeling of methane's thermophysical properties are essential for the design, optimization, and simulation of processes involving its production, processing, storage, transportation, and combustion, as well as for climate change mitigation and a wide range of industrial applications. Among these properties, thermal conductivity is particularly critical, as it supports both experimental measurements and computational analyses required for efficient heat transfer and combustion performance [6–8]. Due to its broad utility as an engineering material, methane is frequently combined with other gases in advanced industrial and chemical processes. Notable examples include methane–carbon dioxide (CO_2) mixtures in biogas combustion [9], methane–carbon monoxide (CO) mixtures for the synthesis of valuable chemicals such as acetic acid [10], methane–tetrafluoromethane (CF_4) mixtures in plasma-enhanced chemical vapor deposition [11], methane–hydrogen (H_2) blends in underground gas storage applications [12], methane–nitrogen (N_2) mixtures in gas separation technologies [13], methane–neon (Ne) mixtures in thick gaseous electron multipliers (THGEM) for radiation detection [14], and methane–argon plasmas used in materials processing [15].

Experimental techniques using specialized instruments and laboratory setups can determine the thermal conductivity of gases and gas mixtures [16]. However, these methods are often complex, time-consuming, and expensive. Additionally, accurate thermal conductivity measurements are typically restricted to specific pressure and temperature ranges. Furthermore, the thermal conductivity of gas mixtures often deviates from a simple linear relationship with the mole fractions of its constituent gases, that is, $\lambda_m \neq \sum x_i \lambda_i$, making it challenging to calculate directly. For gas mixtures composed of molecules with significantly differing polarities, the thermal conductivity of the mixture can exceed the value predicted by a simple mole fraction average [17]. The thermal conductivity of gas mixtures can be significantly influenced by variations in gas density, molecular interactions, and collision frequencies. Estimating and modeling the thermal conductivity of gas mixtures often involve incorporating experimental correlations or theoretical models that account for the influence of gas density, molecular interactions, and collision frequencies. Accurately estimating and modeling the thermal conductivity of gas mixtures often involves incorporating experimental correlations or theoretical models that account for the complex interplay of the aforementioned factors. For low-density gas mixtures, approaches like kinetic theory of gases may be suitable for estimating thermal conductivity. However, dense gas mixtures can exhibit behavior that deviates from ideal gas behavior, necessitating more sophisticated models for accurate thermal conductivity prediction [18]. However, experimental thermal conductivity measurements are crucial for validating theoretical models and correlations. These measurements enhance prediction accuracy and provide valuable insights into the behavior of gas mixtures.

In recent years, such limitations have led to the emergence of data-driven approaches and machine learning (ML) algorithms as powerful alternatives for simulating thermal conductivity.

Table 1 summarizes recent studies [19–22] on modeling and predicting the thermal conductivity of binary methane-based gas mixtures under varying temperatures, pressures, and mole fractions.

1.2 | Advances in Data-Driven Modeling

The development of predictive models for estimating the thermal conductivity of various materials using neural networks has attracted considerable attention in recent years. These data-driven approaches have significantly improved the accuracy and reliability of thermophysical property predictions, while also reducing the time, cost, and resources typically required for experimental measurements [23]. Eslamloueyan and Khademi [24] proposed a three-layer feed-forward neural network (FFNN) to estimate the thermal conductivity of pure gases at atmospheric pressure and a wide range of temperatures based

TABLE 1 | Previous research for predicting the thermal conductivity of methane-based binary gas mixtures.

Ref	Method	x_{CH_4}	P (MPa)	T (K)	Binary mixture
[19]	SAFT-VR Mie equation of state alongside molecular dynamics	0.2413, 0.2592, 0.3043	0.1	300–350	CH_4–CO_2
[20]	Extended corresponding states principle	0.14, 0.25, 0.37	0.7–12	300–425	CH_4–H_2 CH_4–CO_2
[21]	GERG-2008 equation of state (EoS) and Super TRAPP model	0.1–0.9	0.01–100	200–500	CH_4–H_2
[22]	The classical trajectory method using intermolecular potential energy surfaces for the CH_4–CH_4, N_2–N_2, and CH_4–N_2 interactions	0–1	—	70–1200 K	CH_4–N_2

on the critical temperature, critical pressure, and molecular weight. The findings of the study indicate that the proposed FFNN outperforms alternative methods in terms of both accuracy and extrapolation capabilities. Conventional conductivity correlations are typically valid for a limited range of temperatures and substances, whereas the FFNN approach can encompass a broader range of temperatures and materials. In [25], the same authors proposed a neural network architecture consisting of two sequential multilayer perceptrons (MLPs) for predicting the thermal conductivity of binary gas mixtures. The first MLP estimates the thermal conductivity of pure gases based on the critical temperature, critical pressure, molecular weight, and gas temperature. This estimated pure gas thermal conductivity is then used in the second MLP, along with the molecular weights and mole fraction of the lighter component, to predict the thermal conductivity of the binary mixture. Both MLPs exhibit good generalization capabilities, with mean relative error (MRE) and mean squared error (MSE) values of 5.4% and 3.8×10^{-6}, respectively, for the pure gas MLP and 2.2% and 3.3×10^{-6}, respectively, for the binary gas mixture MLP. Farzaneh-Gord et al. [26] developed an MLP neural network to predict the properties of biogas, a mixture of methane and other gases. The network was trained using thermodynamic properties of biogas based on ISO 20765-2 and experimental data. The predictions of the MLP model were compared with those of the equations of state and experimental values. The results demonstrated that the MLP model could accurately calculate output properties such as density, compressibility factor, isochoric heat capacity, isobaric heat capacity, isentropic exponent, internal energy, enthalpy, entropy, Joule–Thomson coefficient, and speed of sound based on a wide range of biogas mixtures and input properties. Naghizadeh et al. [27] presented four advanced intelligent models for thermal conductivity prediction of hydrogen-based binary gas mixtures, including CO, CH_4, and CO_2, based on pressure, temperature, and mole fractions of these components. These algorithms included radial basis function (RBF), cascade forward neural network (CFNN), MLP, and generalized regression neural network (GRNN). Graphical and statistical error analyses demonstrated that the proposed models exhibited strong agreement with the experimental values. Among the proposed models, the GRNN method was identified as the most accurate prediction technique with an root mean square error (RMSE) of 0.00129 and the highest R^2 of 0.9987.

In recent years, convolutional neural networks (CNNs) have emerged as powerful tools for predicting material properties and transport phenomena because of their strong capability of extracting hierarchical and spatially correlated features from structured datasets. Initially, CNN-based approaches were extensively applied in materials science to establish structure property relationships. For instance, Yang et al. [28] employed deep learning (DL) to identify structure property linkages in high-contrast composite materials and demonstrated accurate prediction of effective stiffness directly from simulated microstructural datasets. Similarly, Cecen et al. [29] developed a three-dimensional CNN framework to connect material microstructures with effective material properties, showing that CNN-extracted features significantly improved predictive performance while reducing computational cost. Beyond structural property analysis, CNN models have also been successfully used in transport property prediction. Wu et al. [30] applied DL to predict the effective diffusivity of porous media from structural images and reported significantly lower computational cost compared with conventional lattice Boltzmann simulations. In thermal engineering applications, Wei et al. [31] demonstrated that CNN-based models can accurately predict the effective thermal conductivity of composite materials and porous media, outperforming traditional theoretical correlations. Likewise, Zhu et al. [32] used ML techniques to investigate the relationship between polymer molecular structure and thermal conductivity, enabling efficient screening of high thermal conductivity polymer candidates. More recently, Adam et al. [33] proposed a CNN-based framework inspired by VGG networks for effective thermal conductivity estimation and showed that the model achieved high predictive accuracy while reducing computation time by several orders of magnitude compared with numerical simulations. Additional recent studies by Shen et al. [34] and Liu et al. [35] further confirmed the capability of CNN architectures in accurately estimating effective thermal conductivity in fibrous, particulate, and porous materials with complex microstructures. In addition, Ni et al. [36] demonstrated the effectiveness of DL approaches in predicting thermophysical properties of carbon dioxide under challenging thermodynamic conditions. These studies collectively demonstrate that CNN-based models are highly effective for learning nonlinear relationships between the physical structure and thermophysical behavior. Motivated by these advances, the present work extends the application of CNN modeling to the thermal conductivity prediction of methane binary mixtures.

Unlike previous studies primarily focused on image-based porous or solid material systems, the proposed one-dimensional CNN (1D-CNN) model is designed to capture complex interactions among thermodynamic variables, such as temperature, pressure, and composition, enabling accurate prediction across a wide range of operating conditions relevant to natural gas and energy applications.

1.3 | Research Gap and Novelty of This Study

Existing approaches for predicting the thermal conductivity of CH_4-based binary gas mixtures are mainly based on empirical correlations and theoretical models. Although these methods have been widely applied, they generally require extensive experimental datasets and still struggle to capture the inherently complex and nonlinear interactions among gas components. In recent years, ML techniques have shown promising results across diverse scientific and engineering applications. However, in the field of thermophysical property prediction, most studies have focused on relatively simple ML models, such as linear regression (LR), random forests, or support vector machines (SVMs), while the potential of DL frameworks remains underexplored.

While CNN-based approaches have been increasingly employed for predicting a range of thermophysical properties, their application to the prediction of thermal conductivity in methane-based binary mixtures has received limited attention and remains insufficiently investigated. This represents a clear gap in the literature, as CNN architectures could offer significant advantages in extracting complex features from input parameters such as temperature, pressure, and mole fractions. Specifically, the available data in this field are typically represented as one-dimensional vectors, where the extraction of

local patterns and correlations can be achieved far more effectively through the filtering capability of one-dimensional convolutional layers than with conventional ML techniques.

To bridge this gap, the present study develops and validates a novel DL framework based on 1D-CNNs for the accurate prediction of thermal conductivity in CH_4-based binary gas mixtures. The proposed approach aims to enhance predictive accuracy, reduce reliance on extensive empirical datasets, and provide a robust alternative to conventional ML and theoretical models.

1.4 | Objectives and Scope

The present study is designed to address the challenges of predicting thermal conductivity in methane-based binary gas mixtures by pursuing the following objectives:

1. Data preparation: to collect and preprocess a comprehensive dataset comprising thermal conductivity measurements, temperature, pressure, and mole fractions of CH_4–based binary mixtures and to restructure the data into a one-dimensional format suitable for CNN input.
2. CNN model development: To design and implement a 1D-CNN capable of extracting local feature interactions from the input variables and to optimize its architecture through systematic experimentation with layer configurations and hyperparameters.
3. Training and optimization: to train the CNN using advanced optimization techniques such as root mean square propagation (RMSprop), dropout regularization, and hyperparameter tuning, thereby improving accuracy and reducing overfitting.
4. Model evaluation and benchmarking: to evaluate the predictive performance of the CNN using standard metrics (RMSE, mean absolute error [MAE], mean absolute percentage error [MAPE], and R^2) and to benchmark its accuracy against conventional ML models, including random forest regressor (RFR), support vector regression (SVR) with RBF and linear kernels (SVR-RBF and SVR-linear), LR, and FFNN.
5. Application and validation: to demonstrate the capability of the proposed model in accurately predicting thermal conductivity across a wide range of thermodynamic conditions and compositions for methane-based binary gas mixtures.

Achieving these objectives not only enhances predictive accuracy but also paves the way for implementing the model within industrial design and simulation systems, ranging from gas transmission networks to cryogenic processes.

To provide a comprehensive overview of the methodological steps, the schematic workflow of the present study is illustrated in Figure 1.

1.5 | Organization of the Paper

The remainder of this paper is organized as follows: Section 2 introduces the dataset, outlining the thermophysical variables considered and the preprocessing procedures applied. Section 3 presents the methodology, detailing both the benchmark ML models and the proposed 1D-CNN framework, together with the employed normalization strategies, loss function and optimization scheme, hyperparameter tuning, and architectural design. Section 4 reports and discusses the results, including the performance evaluation of the models and their comparison with reference data available in the literature. Section 5 highlights representative industrial applications where an accurate prediction of thermal conductivity is of critical importance. Finally, Section 6 concludes the study by summarizing the main findings and suggesting possible directions for future research.

2 | Data and Preprocessing

2.1 | Dataset Description

The collected dataset includes thermal conductivity measurements for binary mixtures of CH_4 with seven distinct gases: CO_2, CO, CF_4, H_2, N_2, Ne, and Ar. These measurements are designated as the target output for our neural network model. For the input parameters, the dataset included variables such as temperature, pressure, and mole fractions of the gas mixtures. Table 2 lists the physical and thermodynamic properties of gases used in the present study [37–39].

A comprehensive dataset comprising 1050 data points was gathered from a range of peer-reviewed publications and experimental reports [40–50]. These data points encompass thermal conductivity measurements for various CH_4-based binary gas mixtures under different thermodynamic conditions. A detailed summary of the compiled dataset is presented in Table 3.

It is noteworthy that a rigorous data quality assessment and standardization process were performed to ensure the consistency and compatibility of the data collected from various sources. To this end, all thermodynamic parameters, including temperature (T), pressure (P), and thermal conductivity (λ), were initially converted to SI standards; for instance, temperatures were uniformly standardized to Kelvin (K) and pressures to megapascals (MPa). In cases where experimental conditions required correction for a reference temperature, standard correlations were utilized to verify the data, ensuring that the values were comparable to reference conditions. Furthermore, the compiled data points from different papers and reports were cross compared to identify potential deviations stemming from varying measurement techniques. For this purpose, suspicious values were assessed against the reported error range or uncertainty within their respective sources. Any data points found to be outside the accepted limits of uncertainty were either removed or corrected. This meticulous approach ensured that the final dataset possessed high quality, statistical stability, and reliability for training predictive models.

2.2 | Data Range and Distribution

Table 4 presents the range of key parameters used in this study, including temperature, pressure, mole fraction of components, and the resulting thermal conductivity values of CH_4-based binary gas mixtures. These values range from cryogenic to near-critical conditions (221.32–436.70 K for temperature and

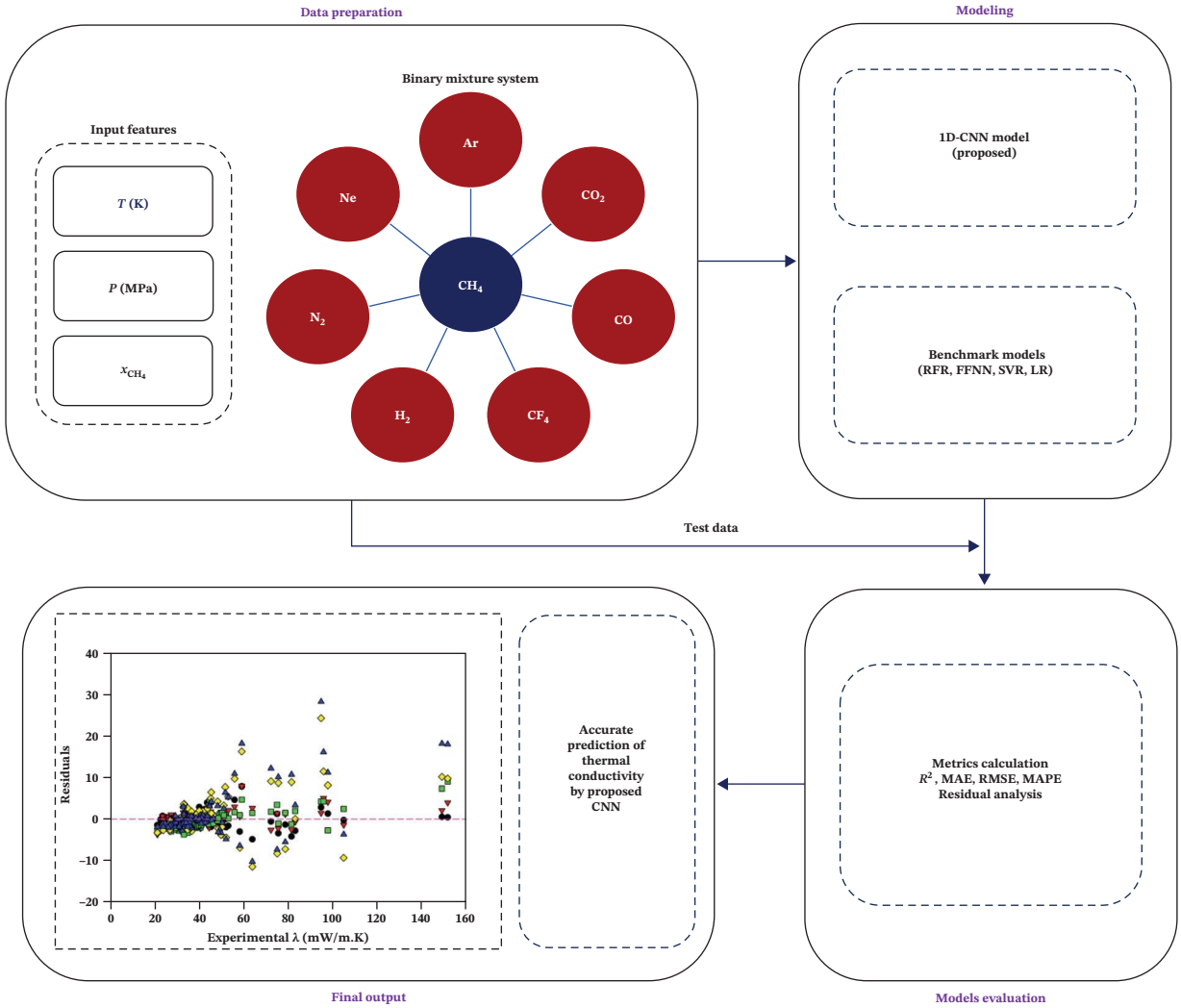

FIGURE 1 | Schematic diagram of the research workflow in the present study.

TABLE 2 | Physical and thermodynamic properties of gases used in CH_4-based binary mixtures.

Gas formula	Molecular weight (g/mol)	Critical temperature (K)	Critical pressure (MPa)	Density (g/L)	Specific heat (C_p, J/mol·K)	Thermal conductivity @300 K (mW/m·K)
CH_4	16.04	190.6	4.6	0.656	35.7	34.4
CO_2	44.01	304.2	7.38	1.977	37.1	16.8
CO	28.01	132.9	3.5	1.25	29.1	25.0
CF_4	88.0	227.6	3.76	3.72	85.0	16.0
H_2	2.02	33.0	1.3	0.0899	28.8	186.6
N_2	28.01	126.2	3.39	1.251	29.1	26.0
Ne	20.18	44.4	2.76	0.9002	27.1	49.4
Ar	39.95	150.9	4.86	1.784	20.8	17.7

0.10–71.14 MPa for pressure). This wide range ensures that the model is trained on diverse conditions, enhancing its robustness and predictive accuracy. The mole fraction varies from pure methane to a pure second component (0.0–1.0), reflecting the full compositional spectrum. The thermal conductivity values range from 19.00 to 151.70 mW/m·K, demonstrating the dataset's broad coverage of heat-transfer behavior across different gas combinations and conditions.

TABLE 3 | CH_4-based binary gas mixture data used for the development of the DL model.

Reference	No. of data	λ (mW/m·K)	x_{CH_4}	P (MPa)	T (K)	Gas mixture
[40]	180	20.96–53.48	0.2493–0.7496	0.724–11.97	300–425	CH_4–CO_2
[41]	62	19–42	0.122–0.902	0.1–9	298.15–308.55	
[42]	48	20.54–35.59	0.2577–0.7861	0.852–6.3	299.55	
[43]	14	19.14–24.45	0.5061	0.217–1.79	228.13–272.07	
[44]	128	25.77–103.9	0.243–0.755	3.38–70.64	335.4–435.6	
[45]	41	28.03–43.32	0.2524–0.7686	0.867–12.2	300.8	CH_4–CO
[46]	153	22.94–82.21	0.267–0.75	0.31–71.14	335.7–436.7	CH_4–CF_4
[47]	50	53.48–151.7	0.1413–0.7733	0.858–8.4	300.65	CH_4–H_2
[48]	171	28.58–52.17	0.2507–0.7494	0.73–15.45	300–425	CH_4–N_2
[49]	11	24.63–36.39	0.5102	0.293–8.73	221.32–271.76	
[43]	55	28.77–38.46	0.2564–0.7707	0.834–8.28	299.5	
[50]	72	37.35–50.65	0.2508–0.7592	1.44–21.68	300.6	CH_4–Ne
[50]	65	21.53–40.71	0.2473–0.7818	0.852–17.57	300.6	CH_4–Ar

TABLE 4 | Range of key parameters used in this study.

Parameter	T (K)	P (MPa)	x_{CO_2}	x_{CO}	x_{CF_4}	x_{H_2}	x_{N_2}	x_{Ne}	x_{Ar}	λ (mW/m·K)
Min	221.32	0.10	0.000	0.00	0.000	0.00	0.00	0.00	0.00	19.00
Max	436.70	71.14	0.878	0.75	0.733	0.86	0.75	0.75	0.75	151.70

A histogram, as shown in Figure 2, was constructed using 20 bins to visualize the distribution of thermal conductivity (in mW/m·K) for the 1050 samples in the dataset. Each bin represents a subrange of λ values and the height of each bar indicates the number of observations within that subrange.

The bin width was approximately 6.64 mW/m·K, calculated as follows:

$$\text{Bin width} = \frac{\lambda_{max} - \lambda_{min}}{\text{Number of bins}}. \quad (1)$$

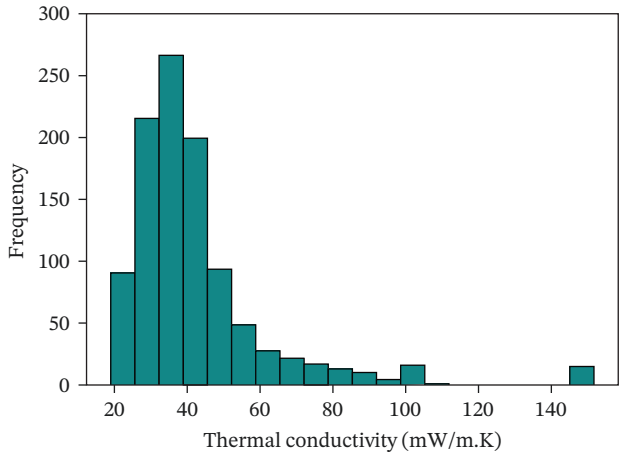

FIGURE 2 | Histogram of target variable (thermal conductivity of CH_4 binary gas mixtures).

Most data points were concentrated in the lower and mid ranges, particularly between 20 and 50 mW/m·K. The bin with the highest frequency was centered approximately around 30–36.6 mW/m·K, indicating that this is the most common range of thermal conductivity in the dataset. The distribution exhibited a positive skew, with a long tail extending toward higher values (above 80 mW/m·K). This suggests that while most gas mixtures have relatively low thermal conductivity, certain compositions or thermodynamic conditions can lead to substantially higher values. This histogram analysis reveals the nonuniform and skewed nature of the thermal conductivity distribution, which should be considered when selecting modeling or regression approaches. This histogram suggests that thermal conductivity values in the gas mixtures tend to cluster around lower values, with relatively fewer instances of high thermal conductivities. The skewness indicates the presence of some gas compositions or thermodynamic conditions that yield an unusually high conductivity.

Figure 3a illustrates the relationship between thermal conductivity and temperature for binary gas mixtures of CH_4 with seven distinct partner gases: CO_2, CO, CF_4, H_2, N_2, Ne, and Ar. In this 2D scatter plot, each data point represents a measured sample, and the color coding distinguishes the gas partner with the highest mole fraction in the mixture. Figure 3a reveals clear temperature-dependent trends for each binary system. Notably, mixtures involving lighter gases such as H_2 tend to exhibit higher thermal conductivity values, especially at elevated temperatures, consistent with their high intrinsic thermal transport properties. Conversely, mixtures with heavier gases, like CF_4 or CO_2, display a comparatively lower thermal conductivity. This visualization

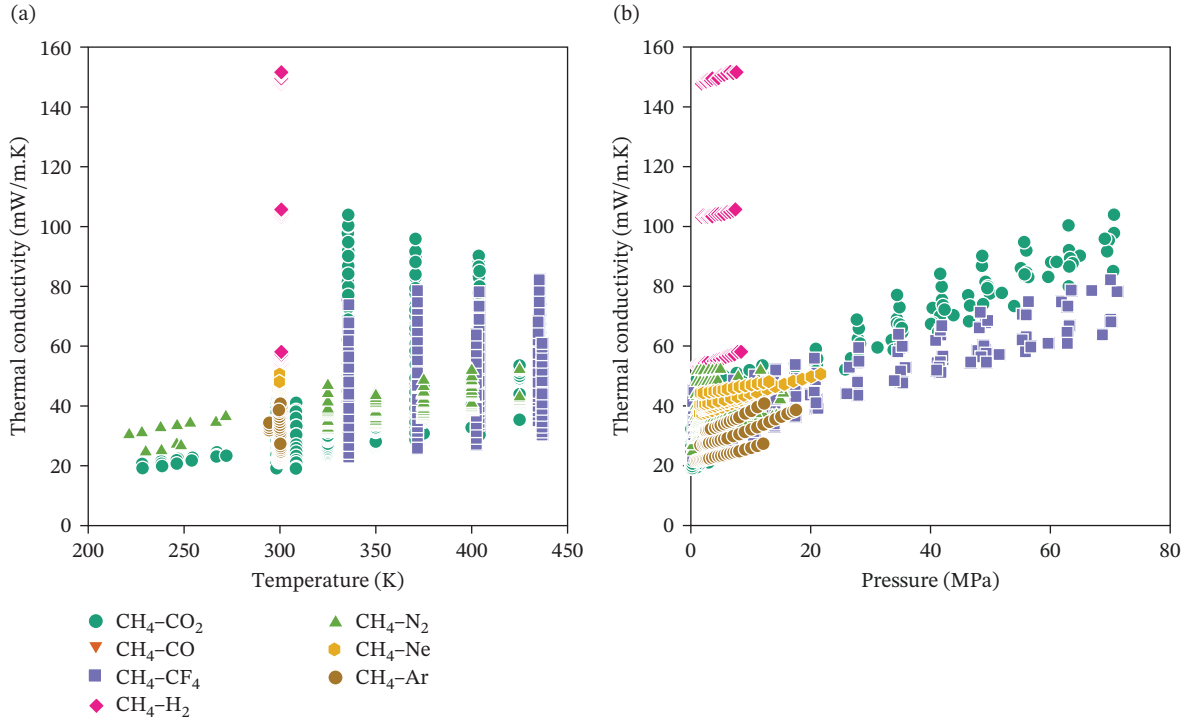

FIGURE 3 | (a) Thermal conductivity vs. temperature. (b) Thermal conductivity vs. pressure for each gas pair.

underscores the nonlinear influence of both temperature and molecular composition on thermal conductivity, highlighting the complexity of modeling such thermophysical properties and the need for robust predictive approaches like CNNs.

Figure 3b illustrates the variation of thermal conductivity with pressure. Each point in the scatter plot represents a unique experimental condition, with color coding corresponding to the dominant gas partner in the mixture. Overall, the trends show that while pressure does influence thermal conductivity, the extent and direction of this effect vary significantly depending on the interacting gas species. For example, mixtures with lighter gases such as H_2 tend to maintain higher thermal conductivity values across a broader pressure range, whereas heavier gases, like CF_4 or CO_2, often exhibit a less pronounced or even decreasing conductivity trend with increasing pressure. These diverse behaviors highlight the complex interplay between molecular interactions, pressure, and thermal transport properties, further justifying the application of nonlinear data-driven models such as CNNs for accurate prediction.

2.3 | Data Normalization and Scaling

To ensure the integrity and reliability of the dataset prior to analysis, a comprehensive preprocessing procedure is carried out. Initially, a thorough examination of the data to identify any potential noise and outliers that could adversely affect subsequent analyses is conducted.

Following the identification of noise and outliers, z-score normalization technique rescales the data based on the mean and standard deviation of each feature. This method transforms the data into a standard normal distribution with a mean of zero and a standard deviation of one. The normalization process is executed according to the following equation [51]:

$$z_v = \frac{v - \mu_v}{\sigma_v},\ v \in \left\{x_{\mathrm{Ar}}, x_{\mathrm{Ne}}, x_{\mathrm{N_2}}, x_{\mathrm{H_2}}, x_{\mathrm{CO}}, x_{\mathrm{CO_2}}, x_{\mathrm{CF_4}},\ T,\ P\right\}, \tag{2}$$

where z_v represents the normalized variable. μ_v and σ_v are the mean and standard deviation of the variable in the training dataset, respectively. They are calculated by:

$$\mu_v = \frac{1}{N}\sum_{i=1}^{N} v_i, \tag{3}$$

$$\sigma_v = \sqrt{\frac{1}{N}\sum_{i=1}^{N}(v_i - \mu_v)^2}. \tag{4}$$

In addition to z-score standardization, which was primarily adopted in this study for scaling the input features, another widely used and effective approach in regression tasks is min–max normalization. This method maps the values of each feature into a predefined interval, typically [0,1], thereby facilitating comparability across variables and often improving interpretability in ML models. The general equation is expressed as [51]:

$$z_v = \frac{v - v_{\min}}{v_{\max} - v_{\min}}, \tag{5}$$

where z_v is the normalized value in interval of [0,1], v is the original value, and $v_{\min}$ and $v_{\max}$ denote the minimum and maximum values of the feature across the dataset, respectively.

In this study, z-score normalization was employed as the primary preprocessing approach for the CNN training data. The min–max normalization method was used solely in comparative experiments, as discussed in Section 4, to assess its influence on the model performance. The combined use of z-score and min–max normalization at different stages of preprocessing allows for a fair comparison of model performance under distinct scaling strategies.

2.4 | Train–Validation–Test Split Strategy

In this study, the dataset was divided into three subsets to ensure robust model development and fair evaluation. Specifically, 80% of the data were allocated for training, enabling the model to learn the underlying functional relationships between temperature, pressure, mole fractions, and thermal conductivity. To prevent overfitting and to guide hyperparameter tuning, 10% of the dataset was used as a validation set, which allowed monitoring of the model's performance during training and the application of techniques such as early stopping and dropout adjustment. Finally, the remaining 10% was reserved as a test set, serving as an entirely unseen dataset for evaluating the generalization ability of the trained models.

This partitioning strategy ensures that model evaluation is unbiased and reflects real-world predictive capability. By employing separate validation and test subsets, the risk of data leakage is minimized, which is crucial for reliable benchmarking of the CNN against conventional ML models. The chosen 80–10–10 split ratio is widely adopted in ML applications, especially when datasets are of moderate size, as it balances the need for sufficient training data with the requirement of maintaining adequate validation and testing samples for robust performance assessment [52].

3 | Methodology

This study utilizes existing experimental data on the thermal conductivity of CH_4-based gas mixtures as the foundation for model development. Based on these measurements, input sequences were generated to construct structured datasets incorporating temperature, pressure, and the mole fractions of seven gases mixed with CH_4. A 1D-CNN model was then developed and validated for the prediction of thermal conductivity. The model architecture and hyperparameters were systematically optimized to enhance the predictive performance. To further investigate the model's behavior, additional analyses were conducted to evaluate the influence of individual input parameters on prediction accuracy.

All models in this study, including the proposed CNN and conventional ML regressors, were developed and implemented using Python. The flexibility and extensive ecosystem of Python libraries, such as TensorFlow and Keras for DL and Scikit-learn for conventional models, enabled efficient model development, training, evaluation, and comparison within a unified programming environment.

3.1 | 1D-CNN Model

In this study, the input variables are organized as a one-dimensional feature vector comprising mole fractions, temperature, and pressure. Although these variables do not form a temporal sequence, 1D-CNN is advantageous because convolutional filters can learn local nonlinear interactions among input features through weight sharing and localized receptive fields. This enables the model to extract compact and informative representations from the thermodynamic input space [53]. Therefore, the proposed 1D-CNN provides an effective framework for capturing localized nonlinear interactions among thermodynamic variables.

Generally, the output of the j-th filter in the l-th convolutional layer, denoted as $y_j^{(l)}$, is calculated as follows:

$$y_j^{(l)}(p) = \sum_{i=1}^{f_l} w_i^{(l,j)} \cdot z_{i+p}^{(l-1)} + b^{(l,j)}, \tag{6}$$

where $z^{(l-1)}$ is the input feature map from the previous layer, f_l is the kernel (filter) size of l-th layer, $w_i^{(i,j)}$ represents the learnable weights of the j-th filter, p is the stride or position index of the input sequence, and $b^{(i,j)}$ is the bias term associated with the j-th filter. This relationship is the basis of the 1D convolution operation and determines how each input feature, T, P, and x_i, is combined to extract relevant patterns.

To introduce nonlinearity and prevent the model from being constrained to linear relationships, the rectified linear unit (ReLU) activation function ($\phi(\cdot)$) was employed after each convolution [54]:

$$z_j^{(l)}(p) = \phi\left(y_j^{(l)}(p)\right) = \max\left(0, y_j^{(l)}(p)\right). \tag{7}$$

This function allows only positive values to pass while setting all negative values to zero. This behavior is crucial as it enables the model to effectively learn the complex, nonlinear interactions present between the thermodynamic variables.

3.2 | Regularization and Overfitting Prevention

To stabilize training and accelerate convergence, batch normalization is applied after each convolutional block. This technique normalizes the intermediate activations by re-centering and re-scaling them according to the statistics of each mini-batch. In each convolutional layer, the pre-activation output ($y_j^{(l)}(p)$) is normalized across the current mini-batch before applying the nonlinear activation function. The batch normalization operation is defined as [55]:

$$\widehat{y}_j^{(l)}(p) = \frac{y_j^{(l)}(p) - \mu_{\text{batch}}}{\sigma_{\text{batch}}}, \tag{8}$$

$$\widetilde{y}_j^{(l)}(p) = \gamma \widehat{y}_j^{(l)}(p) + \beta, \tag{9}$$

$$z_j^{(l)}(p) = \phi\left(\widetilde{y}_j^{(l)}(p)\right), \tag{10}$$

where $y_j^{(l)}(p)$ is linear output of the j-th filter in layer l before normalization, μ_{batch} and σ_{batch} are mean and standard deviation of the mini-batch activations, respectively, $\widehat{y}_j^{(l)}(p)$ is normalized activation, γ and β are learnable scale and shift parameters, $\widetilde{y}_j^{(l)}(p)$ is re-scaled activation after normalization, and $z_j^{(l)}(p)$ is final output after the nonlinear activation function $\phi(\cdot)$.

Dropout randomly deactivates a subset of neurons during training to prevent overfitting and improve generalization [56]. For a given neuron activation, dropout is defined as:

$$\widetilde{h_i} = \begin{cases} h_i & \text{with probability } (1 - p_{\text{drop}}) \\ 0 & \text{with probability } p_{\text{drop}} \end{cases}, \tag{11}$$

where $\widetilde{h_i}$ is activation after applying dropout, h_i is activation of the i-th neuron before dropout. This encourages the model to

learn diverse combinations of features rather than rely excessively on a limited subset of them.

After feature extraction through the convolutional layers, the resulting three-dimensional output is flattened into a one-dimensional feature vector:

$$\boldsymbol{V} = \text{reshape}(\boldsymbol{H}, [1, n_{\text{features}}]), \tag{12}$$

where $\boldsymbol{H}$ denotes the feature matrix and n_{features} represents the total number of extracted features. The final stage is a fully connected (dense) layer that produces the predicted thermal conductivity ($\widehat{\lambda}$), as follows:

$$\widehat{\lambda} = \boldsymbol{W}^T \boldsymbol{V} + b. \tag{13}$$

Equation (13) indicates how all extracted features are linearly combined through the learnable weight matrix $\boldsymbol{W}$ and bias term b to generate the final prediction of thermal conductivity.

In practical terms, the proposed 1D-CNN model processes the input variables, temperature, pressure, and mole fractions of the mixture components, as a one-dimensional signal. As this signal passes through multiple convolutional layers and is filtered at different scales, hidden patterns and dependencies among the variables are extracted. The final dense output layer transforms these learned representations into accurate thermal conductivity predictions. This approach enables the identification of complex, nonlinear relationships without the need for empirical correlations or simplifying assumptions, making it particularly suitable for industrial applications where the system behavior is strongly influenced by variations in composition and pressure.

3.3 | Loss Function and Optimization

The training of the proposed model was performed by minimizing the MSE loss function [53, 54], expressed as:

$$L = \frac{1}{N} \sum_{i=1}^{N} \left(\lambda_i - \widehat{\lambda}_i \right)^2, \tag{14}$$

where N is the total number of training samples, λ_i is the experimental (observed) thermal conductivity of the i-th sample, $\widehat{\lambda}_i$ is the predicted thermal conductivity for the i-th sample, and L is the average squared error across all samples. This loss function provides the error signal required for updating the network parameters.

In this study, RMSprop was chosen as the optimizer due to its ability to maintain a balance between fast convergence and effective handling of complex feature interactions in the dataset. RMSprop has demonstrated an effective and practical optimization algorithm for training deep neural networks like CNNs [52]. It works by adapting the learning rate for each parameter individually using a moving average of the squared gradients, which helps stabilize and accelerate convergence. This prevents oscillations and ensures more stable convergence. For a given parameter vector $\theta = \{w, b\}$ in the CNN (including convolutional and dense layer weights and biases), the gradient of the loss function L with respect to θ at iteration t is denoted as:

$$g_t = \frac{\partial L}{\partial \theta_t}. \tag{15}$$

The core update mechanism involves calculating the moving average of the squared gradients, ω_t, and then using this average to scale the learning rate [57]:

$$\omega_t = \rho \omega_{t-1} + (1 - \rho) g_t^2, \tag{16}$$

$$\theta_{t+1} = \theta_t - \frac{\eta}{\sqrt{\omega} + \varepsilon} g_t. \tag{17}$$

In Equations (16) and (17), $\rho \in [0, 1]$ is the decay rate, η denotes as the global learning rate, and ε is a small constant for stability. In the present study, learning rate and decay rate were set to 10^{-3} and 5×10^{-6}, respectively.

3.4 | Model Architecture

The proposed model in the present study comprises three consecutive Conv1D blocks that incorporate MaxPool1D and dropout layers for robust feature extraction and regularization. This robust convolutional section is then followed by a flattening operation and culminates in a final dense output layer. Figure 4 provides a comprehensive overview, clearly presenting the input feature domain (temperature, pressure, and gas mole fractions), along with the specific hyperparameter configurations for each block, including the number of filters, kernel size, and pooling strides. This schematic is essential for a complete understanding of the model's structure, illustrating how relevant features are progressively extracted and transformed across the network to yield the final predicted value of thermal conductivity (λ).

The final CNN architecture was selected based on a comparative hyperparameter optimization study involving different optimizers, kernel sizes, and dense-layer configurations. Details of the hyperparameter search procedure and the performance of the candidate architectures are provided in Appendix A.

3.5 | Conventional ML Models

To evaluate the effectiveness and superiority of the proposed 1D-CNN framework, a set of conventional ML algorithms were employed as benchmark models. The inclusion of these approaches enables a systematic comparison of the predictive performance of the CNN against well-established techniques frequently applied in thermophysical property prediction. Each algorithm, with its distinct structure and underlying principles, can capture both linear and nonlinear patterns within the dataset. Therefore, benchmarking their results with those of the CNN provides a clearer perspective on the accuracy, generalization capability, and effectiveness of the proposed architecture in extracting complex relationships in methane-based binary gas mixtures. A brief overview of each comparative model and its operating principles is provided in the following sections.

3.5.1 | RFR

RFR is an ensemble learning technique that constructs many independent decision trees during training and outputs the

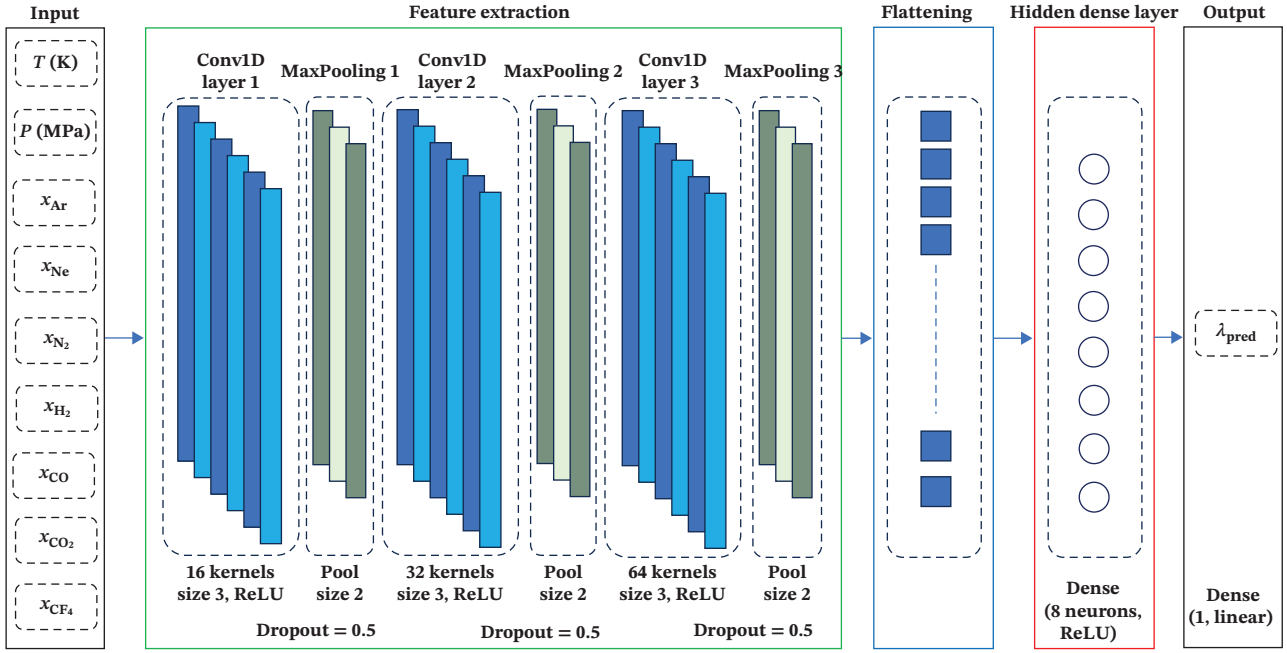

FIGURE 4 | Detailed architecture of the proposed 1D-CNN model.

average of their predictions. Each decision tree is trained on a bootstrapped sample of the dataset, and at each split, a random subset of input features is considered. This combination of bagging (bootstrap aggregation) and random feature selection improves generalization by reducing variance and mitigating overfitting.

For a given normalized input vector of features in this study, $\boldsymbol{z} = \{x_{Ar}, x_{Ne}, x_{N_2}, x_{H_2}, x_{CO}, x_{CO_2}, x_{CF_4}, T, P\}$, the prediction of the m-th decision tree is denoted as $T_m(z)$. The final prediction of the forest, corresponding to the estimated thermal conductivity, $\widehat{\lambda}$, is obtained by averaging across all M trees, as follows:

$$\widehat{\lambda}(z) = \frac{1}{M}\sum_{m=1}^{M} T_m(\boldsymbol{z}), \tag{18}$$

where M is the number of decision trees in the forest, $T_m(z)$ predicts the m-th decision tree, and $\widehat{\lambda}(\boldsymbol{z})$ denotes the final RFR prediction for thermal conductivity.

The robustness of RFR against overfitting stems from its inherent randomness in both data sampling (bootstrapping) and feature selection, combined with the aggregation of multiple uncorrelated trees, which helps reduce variance while maintaining predictive accuracy [58].

3.5.2 | SVR

SVR extends the classical SVM framework to regression problems using an ε-insensitive loss function, which allows small prediction errors to be ignored while maintaining model robustness [59]. The objective of SVR is to determine a regression function with maximum generalization capability by balancing prediction accuracy and model complexity.

For a normalized input vector in this study, that is, $\boldsymbol{z} = \{x_{Ar}, x_{Ne}, x_{N_2}, x_{H_2}, x_{CO}, x_{CO_2}, x_{CF_4}, T, P\}$, the SVR prediction is expressed as:

$$\widehat{\lambda}(\boldsymbol{z}) = \sum_{i=1}^{N} \alpha_i K(\boldsymbol{z_i}, \boldsymbol{z}) + b, \tag{19}$$

where α_i is learned coefficients and b is the bias term. $K(\boldsymbol{z_i}, \boldsymbol{z})$ indicates the kernel function.

In this study, two kernel functions were investigated:

Linear kernel:

$$K(\boldsymbol{z_i}, \boldsymbol{z}) = \boldsymbol{z_i}^T \boldsymbol{z}, \tag{20}$$

which leads to the regression function, as follows:

$$\widehat{\lambda}(\boldsymbol{z}) = w^T \boldsymbol{z} + b. \tag{21}$$

The linear kernel is computationally efficient and suitable when the relationship between inputs and outputs can be approximated by a linear function.

RBF:

$$K(\boldsymbol{z_i}, \boldsymbol{z}) = \exp(-\gamma ||\boldsymbol{z} - \boldsymbol{z_i}||^2), \tag{22}$$

with $\gamma > 0$ controlling the width of the kernel and thereby the flexibility of the regression function. This kernel enables the model to effectively capture complex, nonlinear relationships by transforming the input space into a higher-dimensional feature space, where a LR fit becomes feasible [60]. The flexibility of the RBF kernel makes SVR-RBF particularly suitable for modeling intricate patterns in scientific and engineering datasets.

3.5.3 | LR

LR is one of the most fundamental statistical learning methods used to model the relationship between input variables and a continuous output variable by fitting a linear equation. Its

main advantage lies in its simplicity and interpretability, as the contribution of each input feature to the output can be directly quantified through its regression coefficient. However, LR assumes linear dependence between inputs and the target variable, which limits its applicability in modeling nonlinear relationships. Additionally, it is sensitive to multicollinearity among features and to the presence of outliers [59].

The predicted thermal conductivity can be determined by Equation (21), The model parameters (w and b) are obtained by minimizing the residual sum of squares (RSS) between the observed conductivity values λ_i and the predicted values $\widehat{\lambda}(z_i)$:

$$\min_{w,b} L(w,b) = \sum_{i=1}^{N} (\lambda_i - (w^T z_i + b))^2, \tag{23}$$

where N is the number of training samples.

3.5.4 | FFNN

A FFNN is a class of artificial neural networks in which information flows in one direction only, from the input layer, through one or more hidden layers, to the output layer, without feedback or recurrent connections. FFNNs are universal function approximators and are widely used for modeling complex nonlinear relationships between input features and a continuous target variable. Each neuron in a layer computes a weighted sum of its inputs, adds a bias term, and applies a nonlinear activation function, enabling the network to capture higher-order and nonlinear dependencies that linear models cannot represent.

Compared to LR, FFNNs offer substantially greater flexibility and predictive power for complex systems such as thermophysical property estimation, where interactions between composition, temperature, and pressure are inherently nonlinear. However, this flexibility comes at the cost of increased computational complexity and reduced interpretability, as the learned weights no longer correspond directly to simple physical coefficients. Moreover, FFNNs require careful hyperparameter tuning (e.g., number of layers, number of neurons, and learning rate) and appropriate regularization to avoid overfitting, particularly when training data are limited [61].

In this work, the FFNN maps the input feature vector $\mathbf{z}_i$ to the predicted thermal conductivity $\widehat{\lambda}(\mathbf{z}_i)$ through a sequence of affine transformations and nonlinear activations. For a network with L layers (excluding the input layer), the forward propagation can be expressed as:

For the first hidden layer:

$$\mathbf{h}^{(1)} = \phi\left(\mathbf{W}^{(1)}\mathbf{z}_i + \mathbf{b}^{(1)}\right). \tag{24}$$

For the subsequent hidden layers:

$$\mathbf{h}^{(\ell)} = \phi\left(\mathbf{W}^{(\ell)}\mathbf{h}^{(\ell-1)} + \mathbf{b}^{(\ell)}\right), \ell = 2, \ldots, L-1. \tag{25}$$

The final output layer predicts the thermal conductivity as:

$$\widehat{\lambda}(\mathbf{z}_i) = \mathbf{W}^{(L)}\mathbf{h}^{(L-1)} + \mathbf{b}^{(L)}, \tag{26}$$

where $\mathbf{W}^{(\ell)}$ and $\mathbf{b}^{(\ell)}$ denote the weight matrix and bias vector of the ℓ-th layer, respectively, and $\mathbf{h}^{(\ell)}$ is the hidden representation at layer ℓ; $\phi(\cdot)$ is a nonlinear activation function (e.g., ReLU and tanh). $\widehat{\lambda}(\mathbf{z}_i)$ represents the predicted thermal conductivity corresponding to the input vector.

The model parameters are determined by minimizing the MSE (Equation (14)) between the experimental thermal conductivity values λ_i and the predicted values $\widehat{\lambda}(\mathbf{z}_i)$ over all N training samples.

4 | Results and Discussions

4.1 | Model Evaluation Metrics

To evaluate the performance of the regression models, several standard metrics were employed: MSE, RMSE, MAE, MAPE, and the R^2. These metrics collectively offer a comprehensive assessment of model accuracy and generalization.

MSE and RMSE quantify the average squared and root-squared differences between predicted and actual values, reflecting the overall prediction error [58]:

$$\mathrm{MSE} = \frac{\sum_{i=1}^{N}\left(\lambda_i - \widehat{\lambda}_i\right)^2}{N}, \tag{27}$$

$$\mathrm{RMSE} = \sqrt{\frac{\sum_{i=1}^{N}\left(\lambda_i - \widehat{\lambda}_i\right)^2}{N}}. \tag{28}$$

MAE measures the average magnitude of absolute errors, providing an intuitive sense of prediction accuracy [53]:

$$\mathrm{MAE} = \frac{\sum_{i=1}^{N}\left|\lambda_i - \widehat{\lambda}_i\right|}{N}. \tag{29}$$

MAPE expresses the average prediction error as a percentage of the actual value, providing a scale-independent measure that facilitates comparison across different operating conditions and ranges of thermal conductivity values [53]:

$$\mathrm{MAPE} = \frac{100}{N}\sum_{i=1}^{N}\left|\frac{\lambda_i - \widehat{\lambda}_i}{\lambda_i}\right|. \tag{30}$$

R^2 indicates the proportion of variance in the target variable explained by the model, with values closer to 1 denoting better predictive performance [27]:

$$R^2 = 1 - \frac{\sum_{i=1}^{N}\left(\lambda_i - \widehat{\lambda}_i\right)^2}{\sum_{i=1}^{N}\left(\lambda_i - \overline{\lambda}_i\right)^2}. \tag{31}$$

The selection of evaluation metrics, including MSE, RMSE, MAE, MAPE, and R^2, was motivated by their ability to assess different aspects of model accuracy and performance. In this study, MSE and RMSE were employed due to their high sensitivity to large deviations and their direct connection to error energy as a physically meaningful quantity. RMSE is particularly useful because it

retains the same units as the target variable (λ), enabling direct physical interpretation. MAE reflects the average magnitude of prediction errors, while MAPE provides a relative percentage-based measure of accuracy that is independent of the scale of the target variable. Finally, the R^2 quantifies the proportion of variance explained by the model and is useful for assessing how effectively the model captures the underlying thermophysical behavior. Together, these metrics provide a comprehensive evaluation of the model performance from both statistical and physical perspectives.

To prevent overfitting and ensure stable model training, an early stopping strategy was employed based on the validation loss. The validation loss was monitored at the end of each epoch using a patience value of 20 epochs and a minimum improvement threshold of 1×10^{-4}. In addition, the model was configured to automatically restore the weights corresponding to the epoch with the lowest validation loss.

The training history showed that the validation loss decreased rapidly during the initial training stage and reached its minimum value of 0.00704 at approximately epoch 18. Beyond this point, only minor fluctuations were observed without any meaningful improvement in the validation performance, indicating that the model had effectively converged. Although early stopping was employed throughout the training process, the stopping criterion was not triggered before reaching the maximum epoch limit (400 epochs) because small validation-loss fluctuations persisted. Nevertheless, the weights associated with the minimum validation loss were automatically restored and used for all subsequent evaluations.

Figure 5 presents the complete training history over 400 epochs, illustrating the rapid convergence of both training and validation losses during the early stages of training, followed by a stable plateau with only minor oscillations.

Figure 6a–d presents a comparative evaluation of six regression models, that is, CNN, FFNN, RFR, SVR-RBF, LR, and SVR-Linear, using MAE, RMSE, R^2, and MAPE metric across the training and test datasets. Among these models, CNN achieved

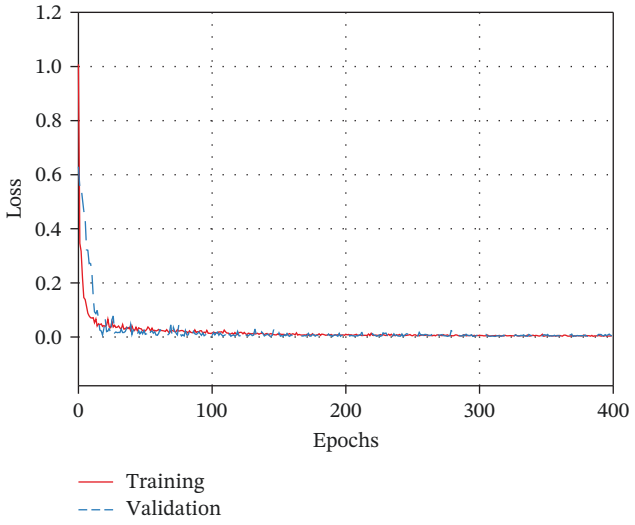

FIGURE 5 | Learning curve of CNN (loss vs. epoch).

the best overall balance between prediction accuracy and generalization performance across all metrics (train: RMSE = 1.25, MAE = 0.70, R^2 = 0.9963, and MAPE = 1.58%; test: RMSE = 1.59, MAE = 0.94, R^2 = 0.9950, and MAPE = 2.02%). These results demonstrate the model's strong generalization ability and its effectiveness in capturing nonlinear relationships within the input features.

The FFNN baseline performs moderately well but remains inferior to the CNN, with slightly higher prediction errors and reduced generalization accuracy (train: RMSE = 1.30, MAE = 0.78, R^2 = 0.9959, and MAPE = 2.02%; test: RMSE = 1.64, MAE = 1.12, R^2 = 0.9938, and MAPE = 2.55%). This performance gap confirms that the convolutional layer provides a more effective local pattern extraction mechanism for this dataset.

The RFR also demonstrates strong predictive capability with limited overfitting (train: RMSE = 1.39, MAE = 0.90, R^2 = 0.9954, and MAPE = 2.21%; test: RMSE = 1.75, MAE = 1.31, R^2 = 0.994, and MAPE = 2.79%), placing it as the second-best traditional ML model.

The SVR-RBF model performs reasonably well but shows noticeably higher errors on the test set (train: RMSE = 1.49, MAE = 1.10, R^2 = 0.9948, and MAPE = 2.32%; test: RMSE = 2.13, MAE = 1.64, R^2 = 0.9911, and MAPE = 3.32%), indicating a weaker ability to generalize fine-scale variations in the data.

In contrast, the linear models, LR and SVR-linear, exhibit the poorest performance, with the highest errors and lowest R^2 scores across both datasets (test LR: RMSE = 4.78, MAE = 2.88, R^2 = 0.955, and MAPE = 6.53%; test SVR-linear: RMSE = 5.53, MAE = 2.96, R^2 = 0.940, and MAPE = 5.40%), clearly indicating underfitting and limited suitability for capturing nonlinear behavior.

Overall, these results highlight the advantage of nonlinear approaches, particularly CNN, in accurately capturing the complex physical relationships governing thermal conductivity in methane-based binary mixtures.

It is important to clarify the role of the convolutional layers within the proposed 1D-CNN architecture. Unlike image-processing CNNs, where convolutional and pooling operations are often employed primarily for dimensionality reduction, the main objective of the CNN in the present study is feature extraction. The convolutional filters act as learnable local operators that capture nonlinear interactions among groups of thermodynamic variables, including temperature, pressure, and mixture composition. Through weight sharing and localized receptive fields, the network learns informative feature representations that emphasize physically relevant relationships while using substantially fewer trainable parameters than a fully connected architecture. Consequently, the benefit of the CNN does not arise from aggressive dimensionality reduction but from its ability to extract structured nonlinear feature interactions before the final regression stage. This interpretation is supported by the comparative results presented in Figure 6, where the CNN consistently outperforms the FFNN baseline despite the modest reduction in feature dimensionality.

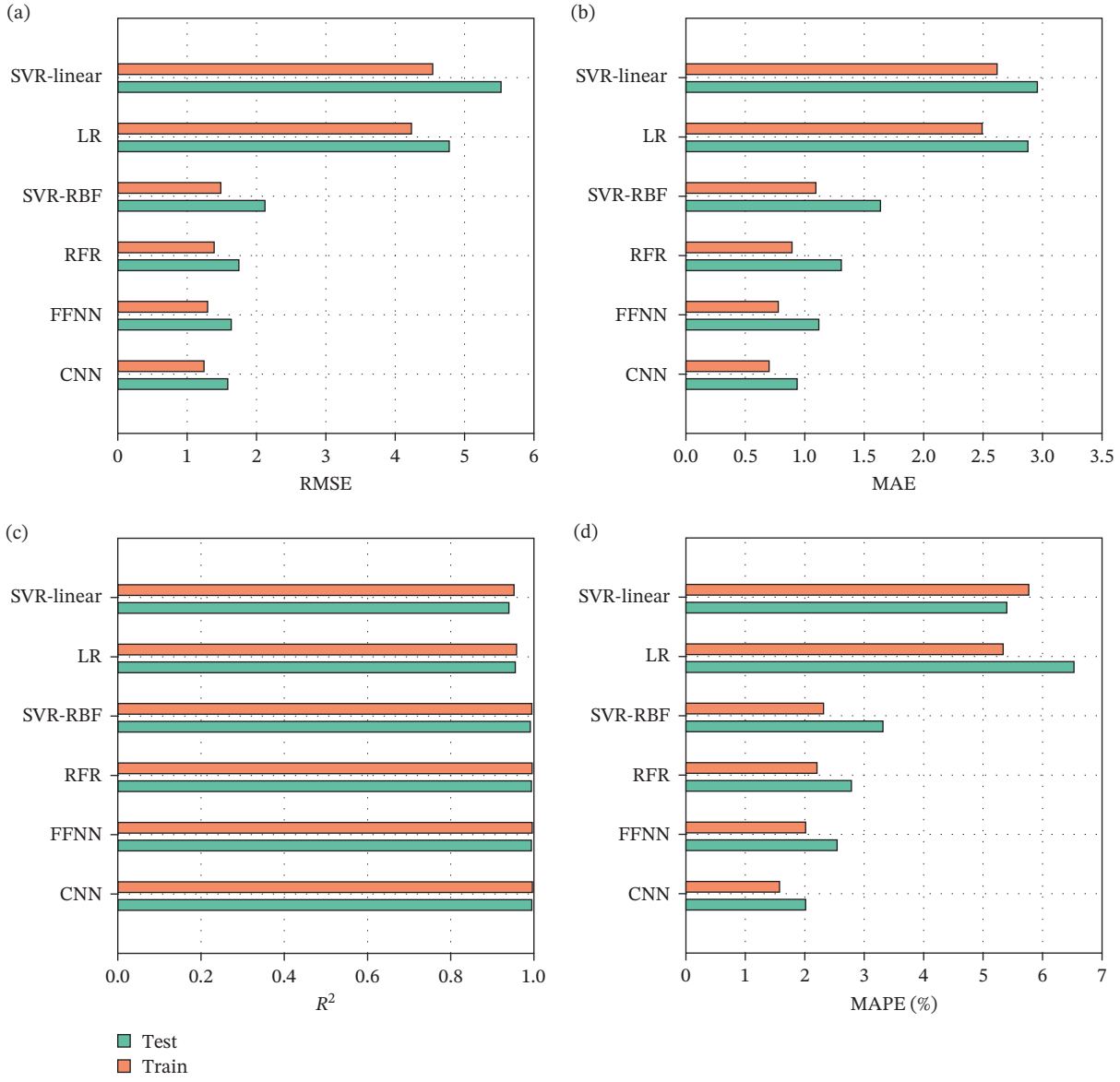

FIGURE 6 | Compare model metrics on train and test data. (a) RMSE, (b) MAE, (c) R^2, and (d) MAPE (%).

4.2 | Comparative Performance of Models

Figure 7 presents a comparative visualization of predicted versus observed thermal conductivity values for four regression models. Each subplot includes a reference line representing the ideal prediction line ($y = x$), allowing for a direct visual assessment of each model's accuracy. The CNN model demonstrates the best performance, with predictions tightly clustered around the diagonal and an R^2 score of 0.995, MAE of 0.94 mW/m·K, and RMSE of 1.59 mW/m·K. RFR also performs well, with an R^2 of 0.994, MAE of 1.31, and RMSE of 1.75, indicating strong consistency. The SVR-RBF model shows moderate alignment, achieving an R^2 of 0.991, but with increased error (MAE = 1.64 and RMSE = 2.13). In contrast, the LR model yields a much lower R^2 of 0.955, with significantly higher MAE (2.88) and RMSE (4.78), reflecting its inability to capture the nonlinear interactions in the data. Figure 7 not only supports the numerical performance results but also visually confirms that CNN and RFR outperform classical models in accurately predicting thermal conductivity in CH_4-based binary gas mixtures.

The superior performance of the CNN model can be explained both from the perspective of thermodynamic data physics and the computational capacity of this architecture to extract nonlinear features.

The model's capability to recognize and reproduce nonlinear dependencies among temperature, pressure, and composition is industrially critical, especially in real systems such as gas transmission networks or LNG cryogenic units, where operational conditions often vary within nonlinear regimes. Having a stable and accurate predictive model in these ranges reduces the need for large safety factors, thereby lowering design costs and enabling more efficient equipment and system optimization while maintaining the desired safety margins.

The dataset in this study comprises variables, such as temperature, pressure, and mole fractions of mixture components, whose relationship with thermal conductivity is often nonlinear, multidimensional, and influenced by intermolecular interactions. The convolutional layers of the CNN enable effective extraction of

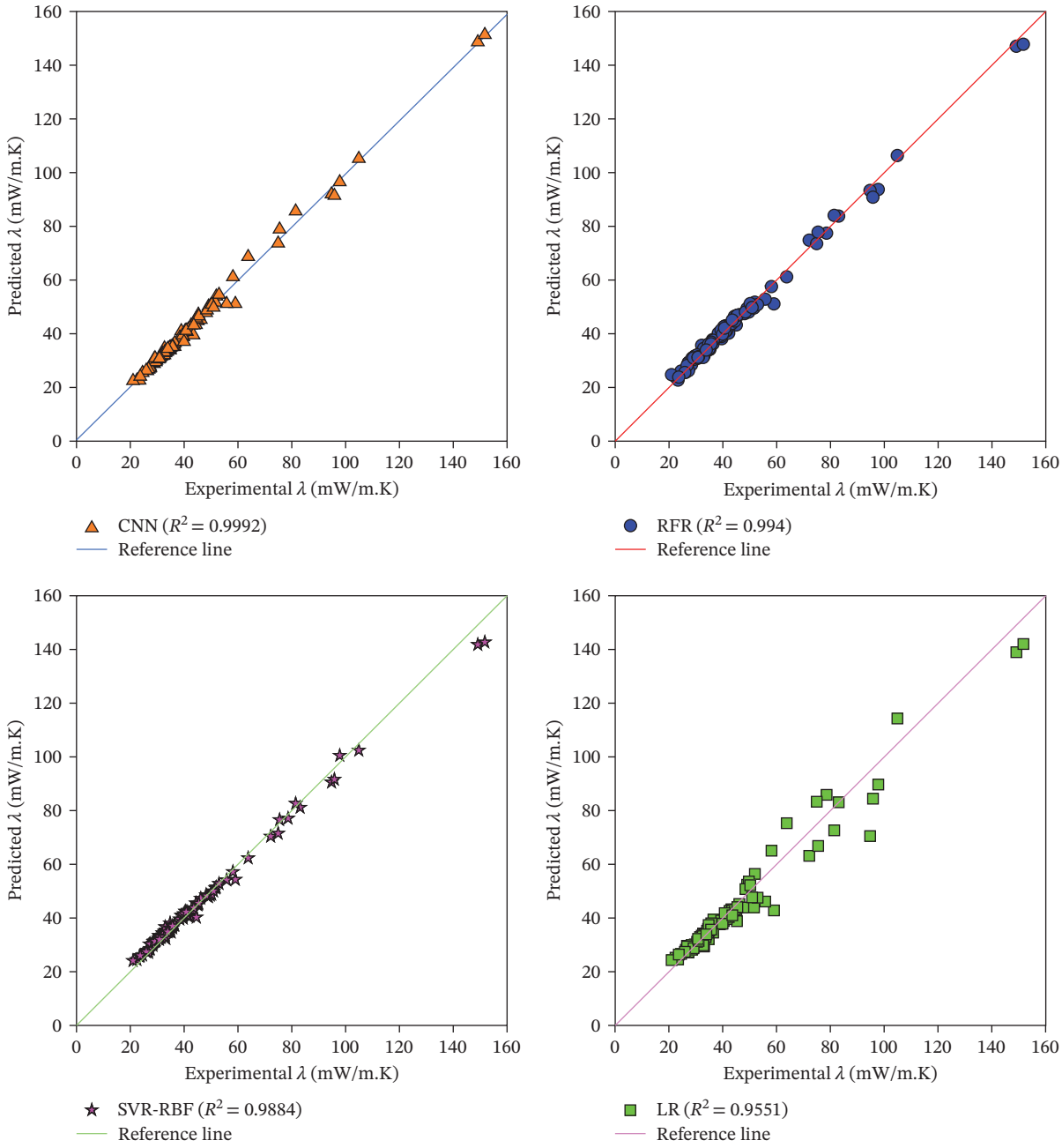

FIGURE 7 | Predicted vs. experimental values.

complex feature interactions from the input vector, allowing the model to learn nonlinear relationships among temperature, composition, and thermal conductivity without requiring explicitly defined physical equations. This enables the model to capture the simultaneous effects of competing factors. For instance, rising temperature decreases density while increasing molecular kinetic energy within a unified framework. Furthermore, nonlinear activation functions (e.g., ReLU) combined with deeper layers allow for hierarchical feature separation and recombination across multiple abstraction levels, a capability that traditional models lack. The outcome of this capacity is a model that achieves very high accuracy and low error in predicting thermal conductivity over a wide range of thermodynamic conditions.

This high level of predictive accuracy also carries a substantial industrial value. For instance, reducing thermal conductivity prediction error led to more precise heat-load estimations and optimal selection of refrigeration capacity in LNG cryogenic equipment, ultimately resulting in energy savings and reduced operating costs. Similarly, in the design of insulation for natural gas pipelines, higher predictive precision minimizes the need for conservative design margins, reducing the insulation weight and material cost. Moreover, by replacing a significant portion of costly laboratory measurements required for λ under various operating conditions, the proposed model can substantially shorten project development timelines and decrease experimental expenses.

4.3 | Error and Residual Analysis

Figure 8 displays the residual plot for the CNN model, illustrating the difference between observed and predicted thermal conductivity values across the test dataset. The residuals are plotted

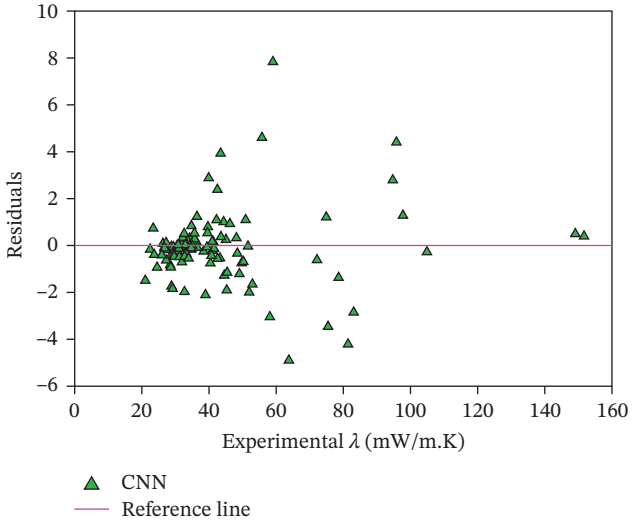

FIGURE 8 | Residual plot of CNN predictions.

against the predicted values to assess the model's bias and variance. The CNN model exhibits a highly favorable residual distribution. Residuals are tightly clustered around the zero-error line, with no clear systematic trend or heteroscedasticity. The maximum residual error observed is approximately ±5.6 mW/m·K, while over 95% of the predictions fall within a narrow error band of ±3 mW/m·K, indicating high consistency. The MAE for the CNN model is 0.94 mW/m·K, and the RMSE is 1.59 mW/m·K, confirming the accuracy reflected in the plot. This uniform residual distribution further validates that the CNN model does not suffer from significant underfitting or overfitting and can generalize well across a diverse range of gas mixture compositions and thermodynamic conditions.

Figure 9 presents a histogram of prediction errors (residuals) for the CNN and RFR models, illustrating the frequency distribution of the differences between the observed and predicted thermal conductivity values. Using 20 bins, Figure 9 clearly shows that the CNN model's residuals are more sharply centered around zero, indicating higher prediction accuracy and less deviation. Specifically, over 80% of CNN's residuals fall within the narrow range of ±2 mW/m·K, and the overall error distribution is symmetric with a peak around 0 mW/m·K. In contrast, the RFR model displays a broader distribution, with a wider spread of residuals and a slightly flatter peak, reflecting greater variability. The CNN model achieved a lower MAE (0.94 mW/m·K) and RMSE (1.59 mW/m·K) compared to RFR (MAE = 1.31 and RMSE = 1.75), and these values are reflected in the relative concentration of the histogram. The visual contrast in error distributions highlights the greater robustness and consistency of the CNN model in capturing the nonlinear relationships within the thermophysical data.

Figure 10 shows the MAE of five predictive models, CNN, RFR, SVR-RBF, SVR-linear, and LR, evaluated across different CH_4-based binary gas mixtures. The chart reveals that the RFR consistently achieves the lowest MAE values for most gas pairs, including CF_4, where it attains an MAE of 1.22 mW/m·K, outperforming even the CNN model, which records an MAE of 1.52 mW/m·K. The SVR-RBF model also performs well, with moderate error values across gases. In contrast, both linear models (SVR-linear and LR) show significantly higher MAEs, indicating their limitations in capturing the nonlinear behavior of thermal conductivity as influenced by molecular composition and thermodynamic conditions. For example, in the CF_4 mixture, LR exhibits a high MAE of 4.32 mW/m·K, more than double that of the top-performing models. This comparison highlights the importance of model selection based on the complexity of the gas interactions and suggests that while DL models like CNN perform strongly overall, ensemble methods such as RFR may offer superior accuracy for specific gas systems.

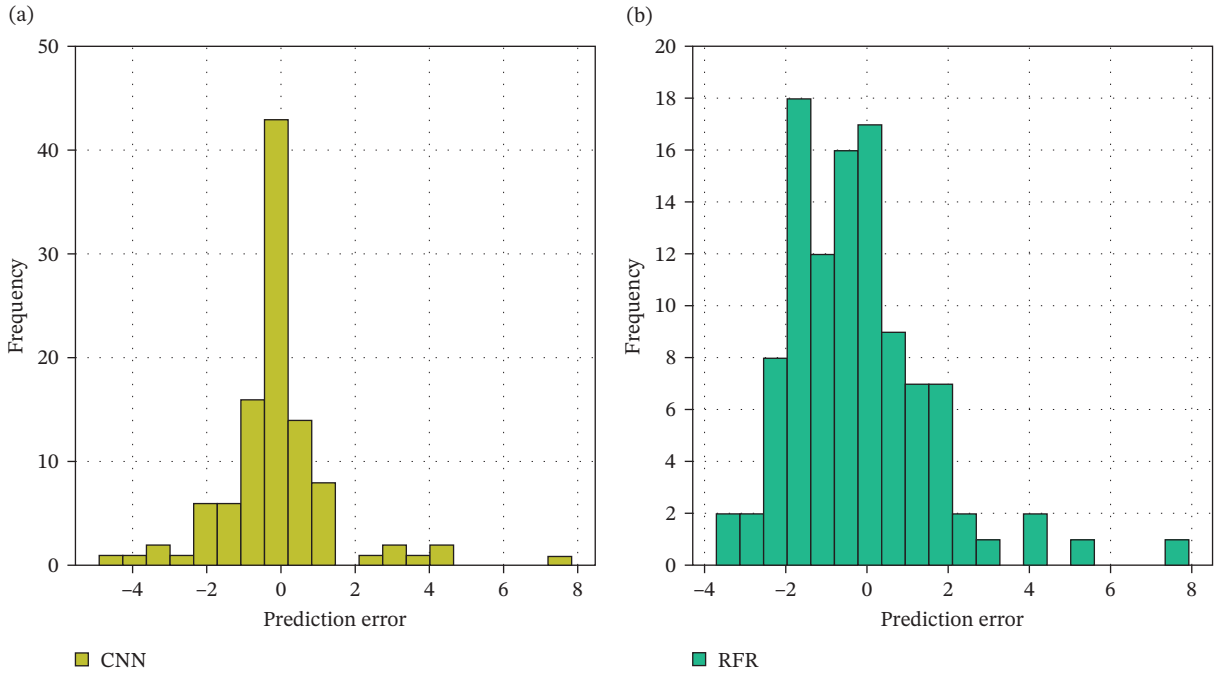

FIGURE 9 | Histogram of prediction errors using 20 bins for (a) CNN and (b) RFR.

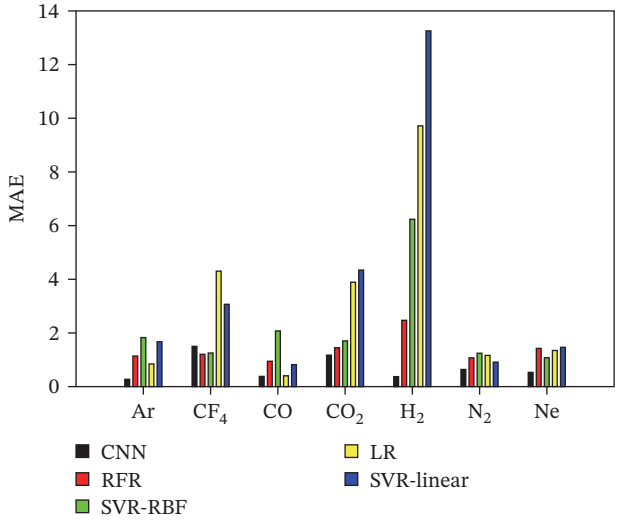

FIGURE 10 | MAE of five predictive models: CNN, RFR, SVR-RBF, SVR-linear, and LR.

Figure 11 presents a series of scatter plots comparing observed and CNN-predicted thermal conductivity values for each CH_4-based binary gas mixture, specifically CO_2, CF_4, N_2, and Ar. Each subplot includes a reference line ($y = x$) to indicate the perfect agreement between predictions and actual measurements. Across all gas mixtures, CNN predictions are tightly clustered around this diagonal line, indicating strong predictive accuracy and minimal systematic bias. Notably, the model achieves exceptionally high R^2 scores of 0.991 for CO_2 and 0.984 for Ar mixtures, underscoring its precise modeling capabilities. Even for CF_4 and N_2 mixtures, where slight dispersion is observed, the CNN maintains high accuracy with R^2 values of 0.978 and 0.960, respectively. This consistent performance across chemically diverse binary systems demonstrates the model's ability to generalize and capture complex thermophysical behavior.

4.4 | Feature Importance and Sensitivity Analysis

Pearson correlation coefficient (r) is a statistical measure that quantifies the strength and direction of the linear relationship between two continuous variables. In the context of this study, it was used to assess the correlation between the predicted thermal conductivity values from the CNN model and the various influencing factors, such as temperature, pressure, and mole fractions of the gases, are involved (CO_2, CO, CF_4, H_2, N_2, Ne, and Ar) [62]:

$$r = \frac{\sum_{i=1}^{N}\left(\lambda_i - \overline{\lambda}\right)\left(z_i - \overline{z}\right)}{\sqrt{\sum_{i=1}^{N}\left(\lambda_i - \overline{\lambda}\right)^2}\sqrt{\sum_{i=1}^{N}\left(z_i - \overline{z}\right)^2}}, \tag{32}$$

where z_i is the influencing parameter for the i-sample.

The coefficient ranges from −1 to 1, where +1 indicates a perfect positive linear correlation, 0 indicates no linear correlation, and –1 indicates a perfect negative linear correlation [62].

A Pearson coefficient close to +1 in this study suggests that the CNN model's predictions strongly align with the influencing parameters, confirming its effectiveness in capturing the underlying physical trends in CH_4-based gas mixtures.

Figure 12 presents the Pearson correlation coefficients between each input variable and the target variable, thermal conductivity, using the complete dataset of CH_4-based binary gas mixtures. Among the input features, temperature (T) shows the strongest positive correlation with thermal conductivity ($r \approx +0.85$), reaffirming its dominant role in governing the heat transport behavior in gases. The mole fraction of hydrogen (x_{H_2}) also displays a high positive correlation ($r \approx +0.77$), which is consistent with the well-known high thermal conductivity of hydrogen. On the other hand, heavier gas components such as CF_4 and CO_2 exhibit moderate negative correlations with thermal conductivity ($r \approx -0.49$ and −0.40, respectively), likely due to their larger molecular weights and lower vibrational mobility, which reduce heat transfer. Other gases, such as N_2, Ne, and Ar, show weak to moderate correlations, both positive and negative. Pressure exhibits only a mild positive correlation ($r \approx +0.14$), indicating a limited direct influence under the studied conditions. These insights not only highlight the physical importance of individual features but also justify the need for complex models capable of capturing their nonlinear and interacting effects such as CNNs.

4.5 | External Validation Against Literature Data

To further evaluate the reliability, physical consistency, and generalization capability of the proposed CNN model, its predictions for thermal conductivity were compared with independent literature-reported data for three representative CH_4-based binary mixtures: CH_4–CO_2, CH_4–H_2, and CH_4–N_2. These systems were selected as external validation cases due to the availability of independent experimental and computational results reported in the literature, thereby providing a robust benchmark for model assessment.

Unlike the training and testing datasets, which originate from the same compiled database, the reference data used in this comparison were obtained from independent studies employing different experimental setups and theoretical approaches [19, 20, 22]. In addition, these datasets include thermodynamic conditions that are not fully identical to those in the training domain, thereby enabling an assessment of the model's extrapolation capability.

The thermal conductivity values were predicted using the trained CNN model under the corresponding thermodynamic conditions of temperature, pressure, and mole fraction and were subsequently compared with literature values digitized from published figures using the PlotDigitizer tool (https://plotdigitizer.com/app).

The comparative results summarized in Table 5 demonstrate strong agreement between the predicted and reference values. The average absolute relative deviation (AARD) across all validation cases is approximately 6.6%, confirming the model's predictive reliability and robustness. This quantitative agreement further indicates that the CNN model can capture the underlying nonlinear thermophysical behavior of methane-based binary mixtures and is not limited to interpolation within the training dataset but also exhibits satisfactory extrapolation performance.

5 | Industrial Applications of Proposed CNN Model

Accurate prediction of the thermal conductivity of methane-based binary gas mixtures has significant industrial implications, as it

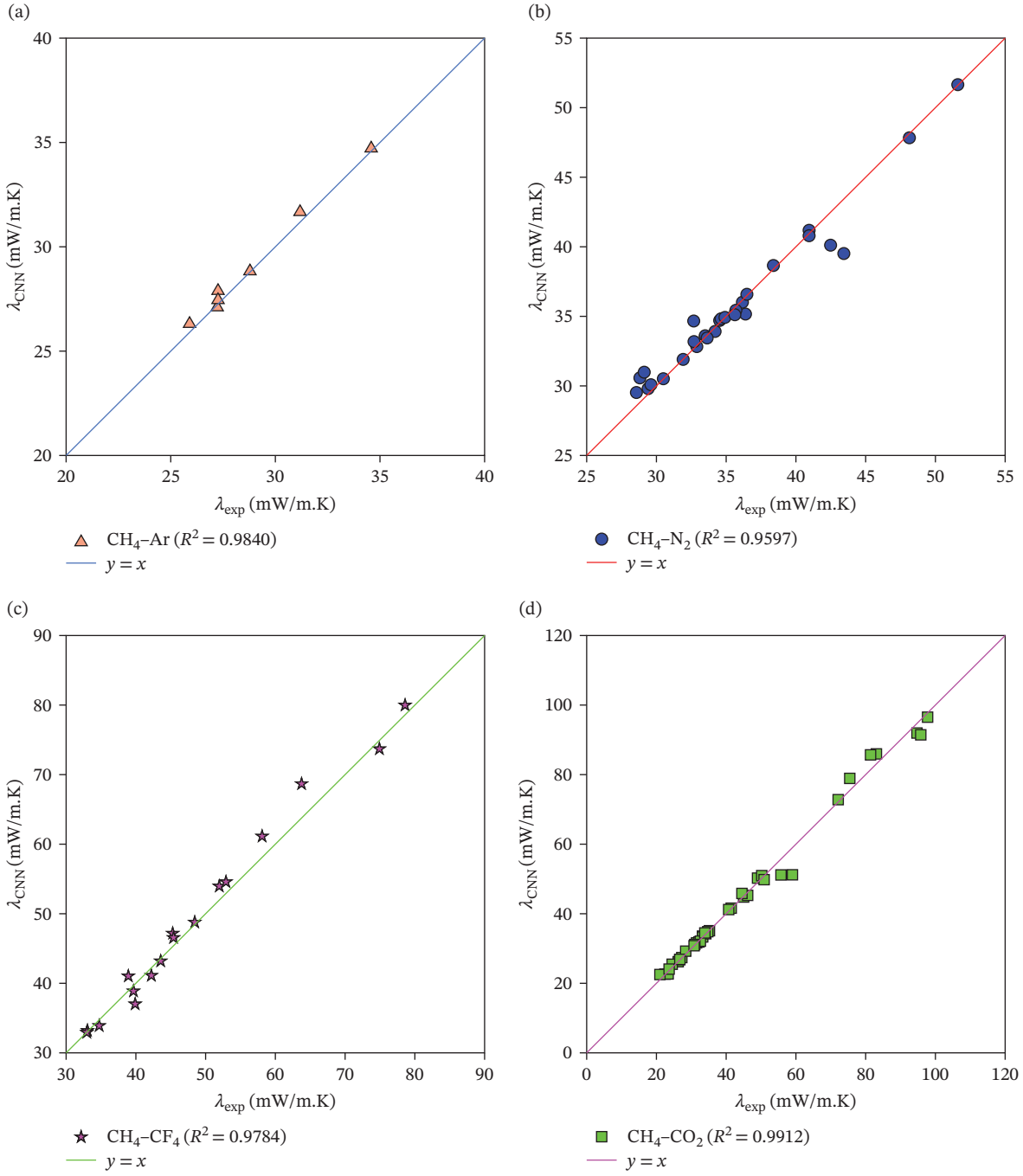

FIGURE 11 | Comparison of observed and CNN-predicted thermal conductivity values for (a) CH_4–Ar, (b) CH_4–N_2, (c) CH_4–CF_4, and (d) CH_4–CO_2 mixtures.

directly affects the design, safety, and efficiency of various thermofluid systems. One of the major challenges in industries is the high cost and time-consuming nature of direct thermal conductivity measurements of gases across a wide range of compositions and operating conditions [20, 21]. The proposed 1D-CNN model addresses this limitation by enabling rapid and accurate predictions of mixture thermal conductivity using only fundamental input data, such as temperature, pressure, and mole fractions, without the need for advanced experimental equipment. This capability significantly reduces laboratory costs, shortens design timelines, and facilitates scenario-based simulations for diverse industrial applications. The representative cases are subsequently discussed briefly, with emphasis on the governing equations in which the role of thermal conductivity (λ) is explicitly highlighted.

- Combustion modeling:

In combustion chambers fueled with methane mixtures, thermal conductivity controls temperature distribution within reactive zones, influencing flame stability and NO_x emissions. The governing energy equation in reactive flow is [63]:

$$\dot{\boldsymbol{Q}}'' = -\lambda \nabla T + \sum \dot{m}_{i,\mathrm{diff}} h_i, \tag{33}$$

where $\dot{\boldsymbol{Q}}''$ is the heat flux vector and $\dot{m}_{i,\mathrm{diff}}$ shows the diffusional heat flux of i-th species. Accurate λ values are needed to simulate flame propagation and optimize burner design.

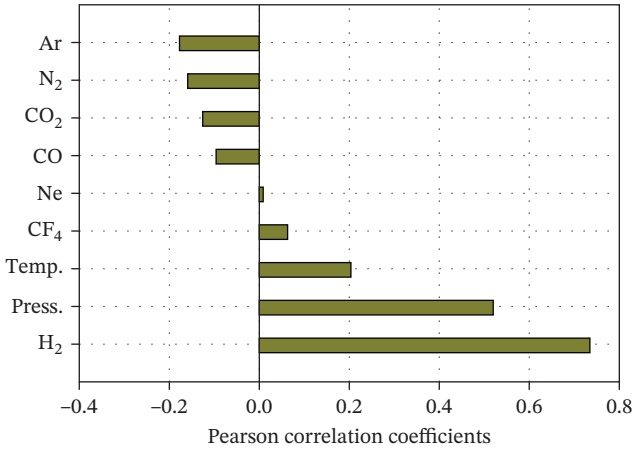

FIGURE 12 | Pearson correlation coefficients between each input variable (mole fractions, temperature, and pressure) and the target variable (thermal conductivity).

In this study, the predictive accuracy of the model (MAE = 0.94 mW/m·K) corresponds to an almost complete reproduction of thermal conductivity behavior under real combustion chamber conditions, enabling precise simulation of temperature profiles and flame stability in industrial design.

- Gas separation and membrane technology:

In membrane-based gas separation processes, thermal conductivity impacts temperature gradients within membranes and modules, which in turn affect transport properties and efficiency. The heat transfer equation for methane reforming through a membrane reactor is given by Lee et al. [64]:

$$\rho C_p \frac{\partial T}{\partial t} + \nabla \cdot (-\lambda \nabla T) + \rho C_p u \cdot \nabla T = Q. \tag{34}$$

In Equation (34), ρC_p is volumetric heat capacity, u is gas velocity, and Q is heat source coming from the reaction. Precise λ values of gas mixtures help in designing efficient thermal management for membrane modules used in CO_2, N_2, and H_2 removal from the gas.

- LNG cryogenic processes:

In cryogenic liquefaction of natural gas, thermal conductivity controls the rate of heat leakage and efficiency of refrigeration cycles. An accurate prediction of the gas mixture's λ is crucial for precisely calculating energy losses and the boil-off rate and selecting appropriate insulation materials to minimize the heat flux [65].

- Natural gas pipeline design and safety:

Gas hydrate formation poses a major operational challenge in natural gas production and transportation, especially in deep-sea pipelines, where low temperatures and high pressures prevail. The stability and growth of hydrates are strongly influenced by thermal conductivity (λ) of methane-based mixtures, since heat transfer governs the local temperature distribution that determines hydrate equilibrium conditions. Inaccurate estimation of λ may lead to erroneous predictions of hydrate onset, which in turn can result in either unnecessary heating and insulation costs or increased risks of flow blockages. Reliable prediction of thermal conductivity, as achieved in this study, provides a powerful tool for improving hydrate management strategies, reducing operational risks, and enhancing both the safety and economic efficiency of pipeline operations [66].

6 | Conclusion

This study presents a novel DL approach utilizing 1D-CNNs for predicting the thermal conductivity of CH_4-based binary gas mixtures. Addressing a critical research gap, the proposed model effectively captures the complex nonlinear interactions between temperature, pressure, and molecular composition, factors that traditional theoretical and empirical models struggle to handle accurately.

A comprehensive dataset comprising 1050 data points from binary mixtures of methane with seven partner gases (CO_2, CO, CF_4, H_2, N_2, Ne, and Ar) was collected and rigorously preprocessed to support robust model training and evaluation. The CNN model demonstrated superior performance compared to conventional ML regressors, including RFR, FFNN, SVR (RBF and linear kernels), and LR. It achieved outstanding predictive accuracy with $R^2 = 0.995$, MAPE = 2.02%, MAE = 0.94 mW/m·K, and RMSE = 1.59 mW/m·K, outperforming all benchmark models on both training and test datasets. Residual analyses and histogram distributions further confirmed the model's generalization capability, consistency, and low bias across a wide range of thermodynamic conditions.

Correlation analysis indicated temperature and hydrogen mole fraction as dominant influencing factors on thermal conductivity, while heavier gases—such as CF_4 and CO_2—had a dampening effect. The model's capacity to learn from such feature interactions underscores the advantage of CNNs in data-driven prediction of thermophysical properties.

In conclusion, this research confirms the effectiveness of CNNs in accurately modeling thermal conductivity in methane-based

TABLE 5 | Comparison of thermal conductivity predictions by the proposed CNN model and literature-reported values for selected CH_4-based binary gas mixtures.

				λ (mW/m·K)			
Gas mixture	x_{CH_4}	T (K)	P (MPa)	**Proposed CNN**	**Literature**	**AARD (%)**	**Reference**
CH_4–CO_2	0.696	300	0.1	21.18	22.86	7.35	[19]
CH_4–H_2	0.372	300	1.85	105.55	103.2	2.28	[20]
CH_4–N_2	0.5	325	1.324	34.81	31.61	10.12	[22]

binary gas systems. The proposed framework holds strong potential for integration into simulation tools and design workflows in chemical engineering and energy systems.

Furthermore, the industrial applications of the proposed model, discussed in detail in Section 5, demonstrate the readiness of this framework for practical deployment in the design and optimization of thermal processes and energy transfer systems across various industrial sectors.

Future studies may explore model generalization to multicomponent mixtures, extend to other transport properties, and explore alternative architectures to further enhance the predictive capabilities and industrial applicability.

Owing to its exceptional accuracy and wide operational coverage across temperature, pressure, and composition domains, the proposed framework is ready for integration into industrial simulation platforms, where it can be directly applied for process design, optimization, and performance evaluation in real-world applications.

Funding

No funding was received for this study.

Conflicts of Interest

The authors declare no conflicts of interest.

Data Availability Statement

The data that support the findings of this study are available from the corresponding author upon reasonable request.

References

1. J. Wang and W. Azam, "Natural Resource Scarcity, Fossil Fuel Energy Consumption, and Total Greenhouse Gas Emissions in Top Emitting Countries," *Geoscience Frontiers* 15, no. 2 (2024): 101757.

2. P. J. Strong, S. Xie, and W. P. Clarke, "Methane as a Resource: Can the Methanotrophs Add Value?" *Environmental Science & Technology* 49, no. 7 (2015): 4001–4018.

3. A. M. Alonso, N. Naval, G. Matute, T. Coosemans, and J. M. Yusta, "Phasing Out Steam Methane Reformers With Water Electrolysis in Producing Renewable Hydrogen and Ammonia: A Case Study Based on the Spanish Energy Markets," *International Journal of Hydrogen Energy* 52 (2024): 1472–1487.

4. R. W. Musamali and Y. M. Isa, "Non-Oxidative Conversion of Methane Into Various Petrochemical Grades over Tunable Tri-Metallic Fe-W-Mo/HZSM-5 Catalyst Systems," *Journal of Saudi Chemical Society* 27, no. 4 (2023): 101657.

5. X. Jiang, D. Mira, and D. L. Cluff, "The Combustion Mitigation of Methane as a Non-CO_2 Greenhouse Gas," *Progress in Energy and Combustion Science* 66 (2018): 176–199.

6. Y. Yan, C. Zhang, G. Wu, S. Feng, and Z. Yang, "Numerical Study on Methane/Air Combustion Characteristics in a Heat-Recirculating Micro Combustor Embedded With Porous Media," *International Journal of Hydrogen Energy* 47, no. 48 (2022): 20999–21012.

7. S. Li, Z. Xu, F. Wang, et al., "Flame Propagation Characteristics and Thermal Radiation Hazards of Methane-Hydrogen-Mixed Cloud Explosion in Unconfined Area: Experiment Research and Theoretical Modeling," *International Journal of Hydrogen Energy* 54 (2024): 1563–1574.

8. M. A. Nemitallah, I. B. Mansir, and M. A. Habib, "Experimental and Numerical Study of Oxy-Methane Flames in a Porous-Plate Reactor Mimicking Membrane Reactor Operation," *International Journal of Energy Research* 43, no. 9 (2019): 7040–7057.

9. N. Hinton and R. Stone, "Laminar Burning Velocity Measurements of Methane and Carbon Dioxide Mixtures (Biogas) Over Wide Ranging Temperatures and Pressures," *Fuel* 116 (2014): 743–750.

10. C. Dong, M. Marinova, K. B. Tayeb, et al., "Direct Photocatalytic Synthesis of Acetic Acid From Methane and CO at Ambient Temperature Using Water as Oxidant," *Journal of the American Chemical Society* 145, no. 2 (2023): 1185–1193.

11. L. G. Jacobsohn, D. F. Franceschini, M. E. H. Maia da Costa, and F. L. Freire Jr., "Structural and Mechanical Characterization of Fluorinated Amorphous-Carbon Films Deposited by Plasma Decomposition of CF_4–CH_4 Gas Mixtures," *Journal of Vacuum Science & Technology A: Vacuum, Surfaces, and Films* 18, no. 5 (2000): 2230–2238.

12. T. A. Buscheck, A. Goodman, G. Lackey, et al., "Underground Storage of Hydrogen and Hydrogen/Methane Mixtures in Porous Reservoirs: Influence of Reservoir Factors and Engineering Choices on Deliverability and Storage Operations," *International Journal of Hydrogen Energy* 49, no. D (2024): 1088–1107.

13. P. Liu, L. Fan, J. Li, et al., "A Microporous Titanium Metal–Organic Framework With Double Nanotraps for Record CH_4/N_2 Separation," *Chemistry of Materials* 36, no. 6 (2024): 2925–2932.

14. M. Cortesi, V. Peskov, G. Bartesaghi, et al., "THGEM Operation in Ne and Ne/CH_4," *Journal of Instrumentation* 4, no. 8 (2009): P08001.

15. M. Baraket, S. G. Walton, Z. Wei, E. H. Lock, J. T. Robinson, and P. Sheehan, "Reduction of Graphene Oxide by Electron Beam Generated Plasmas Produced in Methane/Argon Mixtures," *Carbon* 48, no. 12 (2010): 3382–3390.

16. N. B. Vargaftik, *Handbook of Thermal Conductivity of Liquids and Gases* (CRC Press, 2020).

17. B. E. Poling, J. M. Prausnitz, and J. P. O'Connell, *The Properties of Gases and Liquids*, 5th ed. (McGraw-Hill, 2001).

18. T. H. Chung, M. Ajlan, L. L. Lee, and K. E. Starling, "Generalized Multiparameter Correlation for Nonpolar and Polar Fluid Transport Properties," *Industrial & Engineering Chemistry Research* 27, no. 4 (1988): 671–679.

19. M. Sharifipour and A. Nakhaee, "Prediction of the CH_4–CO_2 Mixture Properties Using SAFT-VR Mie Equation of State and Molecular Dynamics Simulations," *Molecular Physics* 122, no. 17 (2024).

20. F. Li, W. Ma, and X. Zhang, "Prediction of the Thermal Conductivity of $H_2/CO_2/CO/CH_4/H_2O$ Mixtures at High Temperatures and High Pressures Based on the Extended Corresponding States Principle," *International Journal of Thermophysics* 43, no. 8 (2022): 121.

21. A. Hassanpouryouzband, E. Joonaki, K. Edlmann, N. Heinemann, and J. Yang, "Thermodynamic and Transport Properties of Hydrogen Containing Streams," *Scientific Data* 7, no. 1 (2020): 222.

22. R. Hellmann, E. Bich, and V. Vesovic, "Calculation of the Thermal Conductivity of Low-Density CH_4–N_2 Gas Mixtures Using an Improved Kinetic Theory Approach," *The Journal of Chemical Physics* 144, no. 13 (2016): 134301.

23. S. Motahar and S. Sadri, "Applying Artificial Neural Networks to Predict the Enhanced Thermal Conductivity of a Phase Change Material With Dispersed Oxide Nanoparticles," *International Journal of Energy Research* 45, no. 10 (2021): 15092–15109.

24. R. Eslamloueyan and M. H. Khademi, "Estimation of Thermal Conductivity of Pure Gases by Using Artificial Neural Networks," *International Journal of Thermal Sciences* 48, no. 6 (2009): 1094–1101.

25. R. Eslamloueyan and M. H. Khademi, "Using Artificial Neural Networks for Estimation of Thermal Conductivity of Binary Gaseous Mixtures," *Journal of Chemical & Engineering Data* 54, no. 3 (2009): 922–932.

26. M. Farzaneh-Gord, B. Mohseni-Gharyehsafa, A. Arabkoohsar, M. H. Ahmadi, and M. A. Sheremet, "Precise Prediction of Biogas Thermodynamic Properties by Using ANN Algorithm," *Renewable Energy* 147, no. 1 (2020): 179–191.

27. A. Naghizadeh, B. Amiri-Ramsheh, S. Atashrouz, et al., "Modeling Thermal Conductivity of Hydrogen-Based Binary Gaseous Mixtures Using Generalized Regression Neural Network," *International Journal of Hydrogen Energy* 59 (2024): 242–250.

28. Z. Yang, Y. C. Yabansu, R. Al-Bahrani, et al., "Deep Learning Approaches for Mining Structure-Property Linkages in High Contrast Composites From Simulation Datasets," *Computational Materials Science* 151 (2018): 278–287.

29. A. Cecen, H. Dai, Y. C. Yabansu, S. R. Kalidindi, and L. Song, "Material Structure-Property Linkages Using Three-Dimensional Convolutional Neural Networks," *Acta Materialia* 146 (2018): 76–84.

30. H. Wu, W.-Z. Fang, Q. Kang, W.-Q. Tao, and R. Qiao, "Predicting Effective Diffusivity of Porous Media From Images by Deep Learning," *Scientific Reports* 9, no. 1 (2019): 20387.

31. H. Wei, S. Zhao, Q. Rong, and H. Bao, "Predicting the Effective Thermal Conductivities of Composite Materials and Porous Media by Machine Learning Methods," *International Journal of Heat and Mass Transfer* 127 (2018): 908–916.

32. M.-X. Zhu, H.-G. Song, Q.-C. Yu, J.-M. Chen, and H.-Y. Zhang, "Machine-Learning-Driven Discovery of Polymers Molecular Structures With High Thermal Conductivity," *International Journal of Heat and Mass Transfer* 162 (2020): 120381.

33. A. Adam, H. Fang, and X. Li, "Effective Thermal Conductivity Estimation Using a Convolutional Neural Network and Its Application in Topology Optimization," *Energy and AI* 15 (2024): 100310.

34. C. Shen, Q. Sheng, and H. Zhao, "Predicting Effective Thermal Conductivity of Fibrous and Particulate Composite Materials Using Convolutional Neural Network," *Mechanics of Materials* 186 (2023): 104804.

35. P. Liu, Z. Han, W. Wu, Y. Zhao, Y. Song, and M. Chai, "A Developed Convolutional Neural Network Model for Accurately and Stably Predicting Effective Thermal Conductivity of Gradient Porous Ceramic Materials," *International Journal of Heat and Mass Transfer* 225 (2024): 125428.

36. C. Ni, X. Wang, H. Liu, K. Zhang, X. Zheng, and Y. Duan, "Gradient-Harmonizing-Based Deep Learning for Thermophysical Properties of Carbon Dioxide," *Journal of Thermophysics and Heat Transfer* 37, no. 2 (2023): 382–393.

37. D. W. Green and M. Z. Southard, *Perry's Chemical Engineers' Handbook*, 9th ed. (McGraw-Hill, 2019).

38. D. R. Lide, *CRC Handbook of Chemistry and Physics* (CRC Press, 2005, http://www.hbcpnetbase.com Internet Version 2005.

39. C. L. Yaws, *Thermophysical Properties of Chemicals and Hydrocarbons* (William Andrew Publishing, 2008).

40. J. Pátek, J. Klomfar, L. Čapla, and P. Buryan, "Thermal Conductivity of Carbon Dioxide–Methane Mixtures at Temperatures Between 300 and 425 K and at Pressures up to 12 MPa," *International Journal of Thermophysics* 26, no. 3 (2005): 577–592.

41. M. Yorizane, S. Yoshimura, H. Masuoka, and H. Yoshida, "Thermal Conductivities of Binary Gas Mixtures at High Pressures: Nitrogen–Oxygen, Nitrogen–Argon, Carbon Dioxide–Argon, and Carbon Dioxide–Methane," *Industrial & Engineering Chemistry Fundamentals* 22, no. 4 (1983): 458–463.

42. J. Kestin, S. T. Ro, and Y. Nagasaka, "The Thermal Conductivity of Mixtures of Methane With Carbon Dioxide," *Berichte der Bunsengesellschaft für Physikalische Chemie* 86, no. 10 (1982): 945–948.

43. P. L. Christensen and A. Fredenslund, "Thermal Conductivity of Gaseous Mixtures of Methane With Nitrogen and Carbon Dioxide," *Journal of Chemical & Engineering Data* 24, no. 4 (1979): 281–283.

44. B. M. Rosenbaum and G. Thodos, "Thermal Conductivity of Mixtures in the Dense Gaseous State: The Methane–Carbon Dioxide System," *The Journal of Chemical Physics* 51, no. 4 (1969): 1361–1368.

45. N. Imaishi and J. Kestin, "Thermal Conductivity of Methane With Carbon Monoxide," *Physica A: Statistical Mechanics and its Applications* 126, no. 3 (1984): 301–307.

46. B. M. Rosenbaum and G. Thodos, "Thermal Conductivity of Mixtures in the Dense Gaseous State: The Methane–Carbon Tetrafluoride System," *Physica* 37, no. 3 (1967): 442–456.

47. J. Kestin, S. T. Ro, and W. A. Wakeham, "The Transport Properties of Binary Mixtures of Hydrogen With CO, CO_2 and CH_4," *Physica A: Statistical Mechanics and its Applications* 119, no. 3 (1983): 615–638.

48. J. Pátek, J. Klomfar, L. Čapla, and P. Buryan, "Thermal Conductivity of Nitrogen-Methane Mixtures at Temperatures Between 300 and 425 K and at Pressures up to 16 MPa," *International Journal of Thermophysics* 24, no. 4 (2003): 923–935.

49. J. Kestin, Y. Nagasaka, and W. A. Wakeham, "The Thermal Conductivity of Mixtures of Nitrogen With Methane," *Berichte der Bunsengesellschaft für Physikalische Chemie* 86, no. 7 (1982): 632–636.

50. R. Fleeter, J. Kestin, Y. Nagasaka, I. R. Shankland, and W. A. Wakeham, "The Thermal Conductivity of Mixtures of Methane With Argon and Neon," *Physica A: Statistical Mechanics and its Applications* 111, no. 3 (1982): 404–422.

51. Y.-S. Kim, M. K. Kim, N. Fu, J. Liu, J. Wang, and J. Srebric, "Investigating the Impact of Data Normalization Methods on Predicting Electricity Consumption in a Building Using Different Artificial Neural Network Models," *Sustainable Cities and Society* 118 (2025): 105570.

52. I. Goodfellow, Y. Bengio, and A. Courville, *Deep Learning* (MIT Press, 2016).

53. H. Kim, H. Jo, and C. Ryu, "Derivation of Kinetic Parameters and Lignocellulosic Composition From Thermogram of Biomass Pyrolysis Using Convolutional Neural Network," *International Journal of Energy Research* 2024, no. 1 (2024): 6184508.

54. I. Cacciari and A. Ranfagni, "Hands-On Fundamentals of 1D Convolutional Neural Networks—A Tutorial for Beginner Users," *Applied Sciences* 14, no. 18 (2024): 8500.

55. S. Ioffe and C. Szegedy, "Batch Normalization: Accelerating Deep Network Training by Reducing Internal Covariate Shift," in *Proceedings of the 32nd International Conference* (2015): 448–456

56. N. Srivastava, G. Hinton, A. Krizhevsky, I. Sutskever, and R. Salakhutdinov, "Dropout: A Simple Way to Prevent Neural Networks From Overfitting," *Journal of Machine Learning Research* 15 (2014): 1929–1958.

57. H. H. Aghdam and E. J. Heravi, *Guide to Convolutional Neural Networks* (Springer, 2017).

58. M. W. Ahmad, J. Reynolds, and Y. Rezgui, "Predictive Modelling for Solar Thermal Energy Systems: A Comparison of Support Vector Regression, Random Forest, Extra Trees and Regression Trees," *Journal of Cleaner Production* 203 (2018): 810–821.

59. A. Afzal, S. Alshahrani, A. Alrobaian, A. Buradi, and S. A. Khan, "Power Plant Energy Predictions Based on Thermal Factors Using Ridge and Support Vector Regressor Algorithms," *Energies* 14, no. 21 (2021): 7254.

60. H. Azimi, H. Bonakdari, and I. Ebtehaj, "Design of Radial Basis Function-Based Support Vector Regression in Predicting the Discharge

Coefficient of a Side Weir in a Trapezoidal Channel," *Applied Water Science* 9, no. 4 (2019): 78.

61. N. Aftabi, N. Moradi, and F. Mahroo, "Feed-Forward Neural Networks as a Mixed-Integer Program," *Engineering With Computers* 41, no. 4 (2025): 2411–2429.

62. J. J. Berman, "Chapter 4—Understanding Your Data," in *Data Simplification*, (Morgan Kaufmann, 2016): 135–187.

63. S. R. Turns, *Introduction to Combustion*, third ed. (McGraw-Hill, 1996).

64. B. Lee, S. Lee, and H. Lim, "Numerical Modeling Studies for Methane Dry Reforming in a Membrane Reactor," *Journal of Natural Gas Science and Engineering* 34 (2016): 1251–1261.

65. R. F. Barron, "Advances in Cryogenic Principles," in *Cryogenic Engineering*, (Springer, 2007): 105–119.

66. S. Mokhatab and W. A. Poe, *Handbook of Natural Gas Transmission and Processing*, third ed. (Gulf Professional Publishing, 2012).

Appendix A. Hyperparameter Optimization

To determine an appropriate CNN architecture, a series of hyperparameter optimization experiments were conducted using the validation dataset. The investigated hyperparameters included the optimizer type, convolution kernel size, and network depth. The objective was to identify a model that achieved high predictive accuracy while maintaining architectural simplicity and minimizing overfitting.

Two widely used optimizers, Adam and RMSprop, were evaluated. Although Adam is commonly employed in DL applications, RMSprop consistently yielded lower validation errors for the present dataset. The convolution kernel size was varied among 2, 3, and 5. A kernel size of 3 provided the most favorable balance between feature extraction capability and model complexity, whereas smaller kernels were unable to adequately capture local feature interactions and larger kernels did not produce additional accuracy gains.

The effect of network depth was also examined by comparing architectures with one and two dense layers. The results indicated that a single dense layer was sufficient for mapping the extracted convolutional features to thermal conductivity. Increasing the number of dense layers led to only marginal performance changes while introducing additional trainable parameters and a greater risk of overfitting.

Based on the validation results summarized in Table A1, the final CNN architecture employing RMSprop, a kernel size of 3, and one dense layer was selected for subsequent training and testing. The selected architecture subsequently achieved a test RMSE of 1.59 mW/m·K.

TABLE A1 | Hyperparameter optimization results for the evaluated CNN configurations.

Configuration	Optimizer	Kernel size	Dense layers	Validation RMSE
Selected CNN	RMSprop	3	1	1.33
Alternative 1	Adam	3	1	1.46
Alternative 2	RMSprop	2	1	1.55
Alternative 3	RMSprop	5	2	1.40